

Radio pulsar polarization as a coherent sum of orthogonal proper mode waves

J. Dyks

Nicolaus Copernicus Astronomical Center, Rabiańska 8, 87-100, Toruń, Poland

Accepted Received ...; in original form 2018 Dec 27

ABSTRACT

Radio pulsar polarization exhibits a number of complex phenomena that are classified into the realm of ‘beyond the rotating vector model’ (RVM). It is shown that these effects can be understood in geometrical terms, as a result of coherent and quasi-coherent addition of elliptically polarized natural mode waves. The coherent summation implies that the observed tracks of polarization angle (PA) do not always correspond to the natural propagation mode (NPM) waves. Instead, they are statistical average of coherent sum of the NPM waves, and can be observed at any (and frequency-dependent) distance from the natural modes. Therefore, the observed tracks of PA can wander arbitrarily far from the RVM, and may be non-orthogonal. For equal amplitudes of the NPM waves two pairs of orthogonal polarization modes (OPMs), displaced by 45°, can be observed, depending on the width of lag distribution. Observed pulsar polarization mainly results from two independent effects: the change of mode amplitude ratio and the change of phase lag. In the core region both effects are superposed on each other, which can produce so complex behaviour as observed in the cores of PSR B1933+16, B1237+25 and J0437–4715. Change of the phase lag with frequency ν is mostly responsible for the observed strong evolution of these features with ν . The coherent addition of orthogonal natural waves is a useful interpretive tool for the observed radio pulsar polarization.

Key words: pulsars: general – pulsars: individual: PSR J0437–4715 – pulsars: individual: PSR B1237+25 – pulsars: individual: PSR B1919+21 – pulsars: individual: PSR B1933+16 – radiation mechanisms: non-thermal.

1 INTRODUCTION

Radio pulsars exhibit a wealth of polarization phenomena that have been studied for half a century. However, both the regular polarization properties as well as peculiar effects escape thorough understanding. The regular behaviour includes the appearance of two orthogonal polarization modes (OPMs) and transitions (jumps) between these OPMs at several longitudes in a pulse profile. Peculiar effects are numerous and involve strong deformations of polarization angle (PA) curve, especially at the central (core) profile components (Smith et al. 2013, hereafter SRM13; Mitra et al. 2015, hereafter MAR15) as well as ‘half orthogonal’ PA jumps (Everett & Weisberg 2001; MAR15). The research on the subject includes the analysis of the natural propagation wave modes in magnetised plasma (Melrose 1979; Lyubarskii & Petrova 1999; Rafat et al. 2018), curvature radiation properties (Gangadhara 2010), numerical polarized ray tracing (Wang et al. 2010), coherent (Edwards & Stappers 2004) and noncoherent deconvolution into separate modes (Mel-

rose et al. 2006; McKinnon 2003), instrumental noise effects (McKinnon & Stinebring 2000) as well as interstellar propagation effects (Karastergiou 2009; McKinnon & Stinebring 1998). This is accompanied by a steady increase in the available polarization data of ever increasing quality (eg. recently Rankin et al. 2017; Brinkman et al. 2018).

In this paper I develop the polarization model based on coherent addition of waves in two orthogonal propagation modes (Dyks 2017, hereafter D17). The extended model offers a more general nature of the observed PA tracks and solves several interpretive obstacles that have appeared in D17.

In Sect. 2 I describe observations and modelling hints that inspired this study. These suggest the importance of equal modal amplitude in pulsar signal, so in Sect. 3 I describe a special-case model based on coherent addition of linearly polarized waves of equal amplitude. The model is used to interpret observations in Sect. 4, which is a good opportunity to present the model properties. Since the equal modal amplitudes may be driven by a circularly polarized signal,

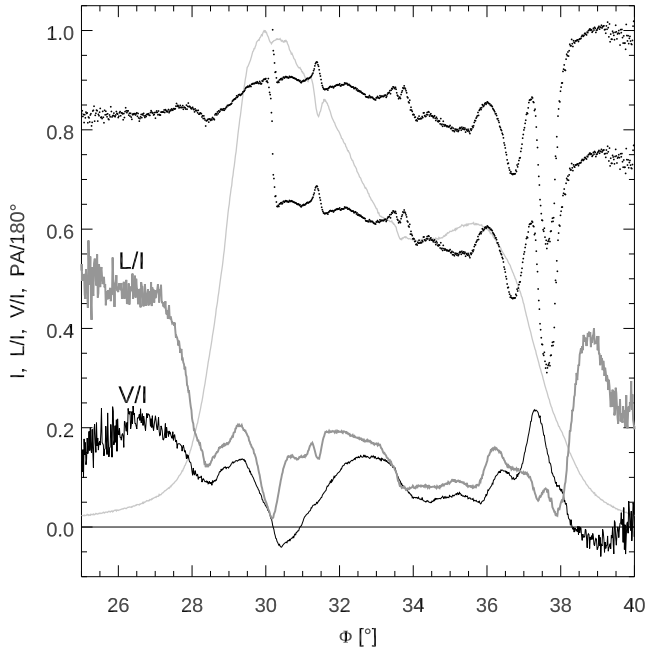


Figure 1. Polarisation characteristics of PSR B1919+21 at 352 MHz, after MAR15. The dots present the PA in units of 180° , plotted at an arbitrary absolute value. The PA is plotted twice at a distance of 45° (equivalent to 0.25). Light grey intensity profile is shown in the background for reference. The PA jump near $\Phi = 30^\circ$ is nearly perfectly equal to 45° . The circular polarization fraction (bottom black solid line) passes through zero at the jump and L/I (grey) is minimal.

in Sect. 5 the model based on the circular feeding is extended into a ‘birefringent filter pair’ model which is applied to the issue of why the OPMs are so often observed nearly equal. Section 6 describes the double, ie. convolved or mixed nature of the polarization observed in the core profile region such as demonstrated by the case of PSR J0437–4715. The equal amplitudes and linear polarization of the natural mode waves cause some interpretive problems (described in Sect. 6.2), therefore, the ellipticity and different amplitudes of the modal waves are taken into account in a more general model described in Sect. 7.1. A glimpse of the properties of the model’s parameter space is given in Sect. 7.2. Interpretive capabilities of the model are presented in Sect. 7.6 where the PA loop of PSR B1933+16 is modelled at two frequencies.

2 INSPIRING OBSERVATIONS AND MODELLING HINTS

2.1 Observations

Fig. 1 presents the polarized profile of PSR B1919+21 as observed by MAR15. The profile exhibits a sharp 45° PA jump near the maximum flux in the profile. The PA is plotted twice at a separation of 45° which shows that the change of PA at the jump is near perfectly equal to 45° . This may seem not strange given that the jump coincides with deep minimum in the linear polarization fraction L/I and with a sign change of the circular polarization fraction V/I . These are trademark features of the equal modal power, and are

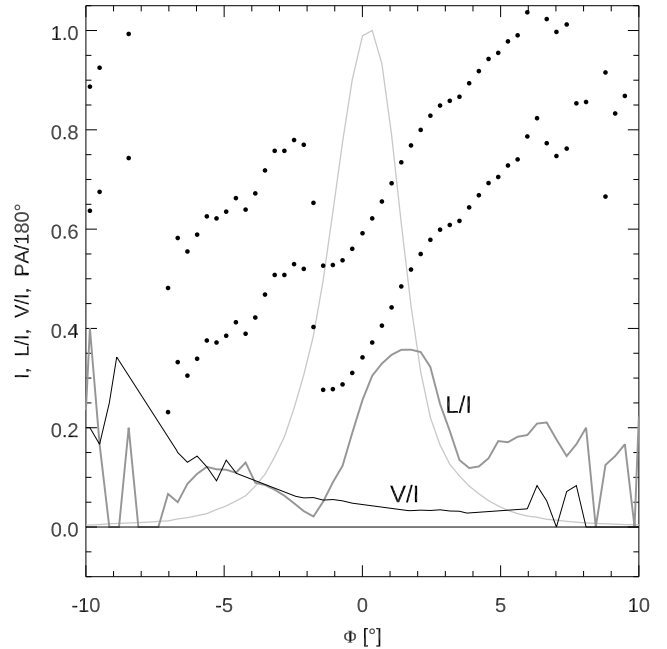


Figure 2. Polarization characteristics of PSR B0823+26 at 1.4 GHz, after Everett & Weisberg (2001). The same convention as in Fig. 1 is used, with the PA (dots) plotted twice at a distance of 45° . The 45° jump at $\Phi \approx 2^\circ$ coincides with a minimum in L/I , but the circular polarization fraction (black solid) is not affected.

frequently observed at the regular OPM jumps. However, after some wiggling on the trailing side of the profile, at the pulse longitude $\Phi = 37.5^\circ$ the PA makes another 45° downward transition, quickly followed by a more standard 90° upward OPM jump at $\Phi = 38^\circ$.

When moved up by 45° , the displaced central PA segment (between $\Phi = 30^\circ$ and 37°) provides roughly rectilinear interpolation between the PA observed outside of the segment. This suggests that the PA stays at the 45° distance through most of the pulse window, and there must be some geometric reason for this. The 45° shift seems to exist despite a clearly nonzero level of both L/I and V/I . Fig. 18 in MAR15 shows that a chaotic multitude of different PA values are observed within the displaced-PA interval of pulse longitude.

As can be seen in Fig. 2, based on Fig. 7 in Everett & Weisberg (2001), PSR B0823+26 also shows a 45° jump which is coincident with a minimum in L/I . In this case, however, the profile of V/I does not seem to be affected by the phenomenon.

In D17 the half-orthogonal PA jump has been interpreted as a sudden narrowing of a phase delay distribution, with the delay measured between two linearly polarized waves, supposedly representing the waves of natural propagation modes. The small delays imply coherent addition of waves, which ensures the 45° PA jump as soon as the waves have equal amplitudes. However, this rises interesting questions. First, what makes the amplitudes equal, and second – having two pairs of orthogonal PA values off at 45° – which pair coincides with the PA of the supposedly quasi linear¹

¹ Hereafter, the terms ‘linear’ or ‘circular’, when referring to sig-

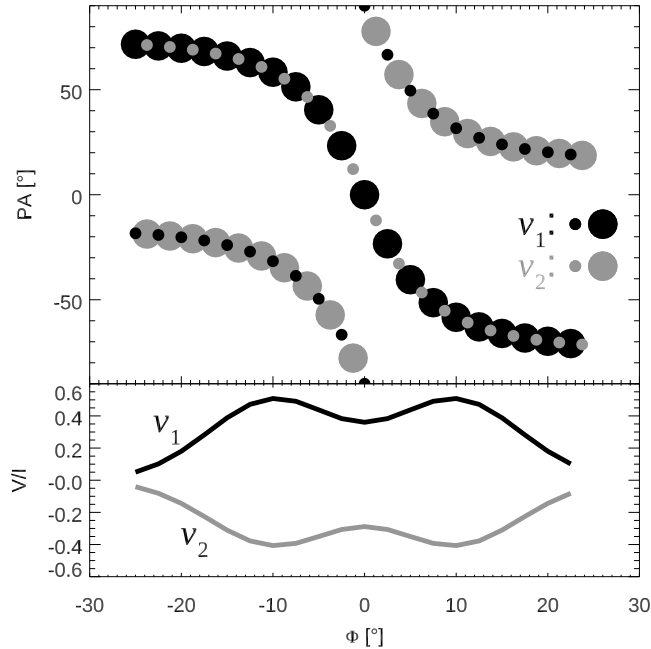


Figure 3. Cartoon presentation of the primary mode exchange effect, after Figs. 4 and 7 of Young & Rankin (2012). The black and grey colors refer to different frequencies ν_1 and ν_2 . The size of points represents the strength of modal track. With the change of ν the strongest mode appears at orthogonal position (90° off) and the observed V changes sign to opposite (bottom panel).

natural polarization modes? Below I will confirm the idea of the lag-distribution narrowing, however, the identification of the modes will be shown to depend on whether equal modal amplitudes can be sustained in pulsar signal.

Another type of interesting polarization phenomenon is the exchange of the observed modal power with increasing frequency ν . This is well illustrated in Figs. 4 and 5 of Young and Rankin (2012) where single pulse PA distributions are shown at two frequencies for PSR B0301+19 and B1133+16.² In Fig. 3 I show a cartoon representation of this effect. The PA distribution in each pulsar reveals two enhanced PA tracks that follow a pair of well defined rotating vector model (RVM) curves, with each PA track apparently representing a different OPM. However, the primary (ie. brighter) mode track at 327 MHz becomes the secondary (fainter) track at 1.4 GHz. According to the authors, the data were corrected for the interstellar Faraday rotation, various instrumental effects and dispersion. Moreover, the apparent replacement of the modal power is confirmed by a probably concurrent change in the sign of V . The power of the observed OPMs is then partially separated not only in pulse longitude and drift phase (Edwards & Stappers 2003; Rankin & Ramachandran 2003; Edwards 2004), but also in the spectral domain (Noutsos et al. 2015). This may seem to be natural, because the modes are generally expected to have different refraction indices, each with different dependence on ν , which implies a ν -dependent phase lag between the modal waves. In the model of D17, however, any changes

nals, waves or modes, should always be understood as ‘linearly polarized’ and ‘circularly polarized’, respectively.

² The authors do not comment on this exchange at all.

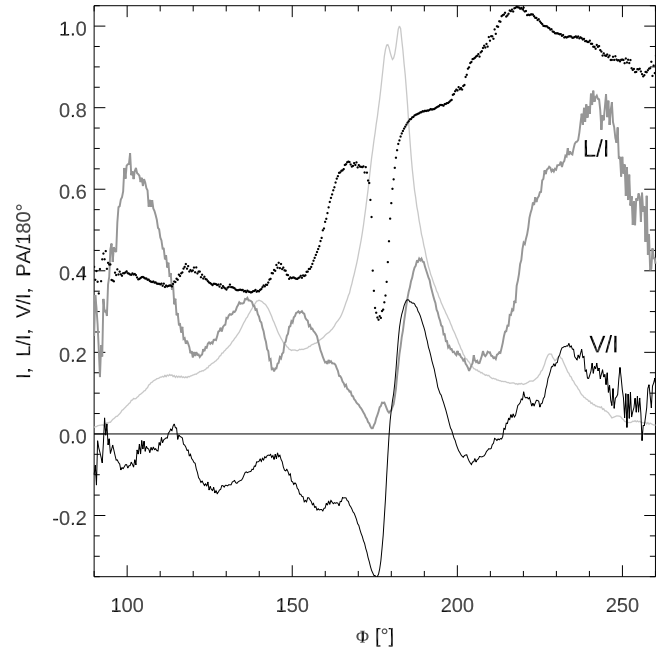


Figure 4. Polarization characteristics of J0437–4715 at 660 MHz, after Navarro et al. (1997). Graphical convention is the same as in Fig. 1, except from that the PA (dots) is plotted once. The profile of L/I has two nearby minima in the profile center ($\Phi = 175^\circ$). The right minimum coincides with the handedness change of V . The left one occurs at high V/I . Both minima correspond to OPM jumps visible in the PA (the right one has magnitude close to 90°).

of the phase lag could not affect the ratio of modal power. This lack of flexibility makes the ν -related considerations difficult and calls for the model extension.

Another type of insightful polarization effects are the distortions and bifurcations of polarization angle tracks, especially those observed within the central (core) components of pulsars such as PSR B1237+25 (SRM13), B1933+16 (Mitra et al. 2016, hereafter MRA16), B1857–26 (Mitra & Rankin 2008), and B1839+09 (Hankins & Rankin 2010). All these phenomena reveal clear signatures of their coherent origin: they have maxima of $|V|$ coincident with minima of L/I . The loop-like PA distortion of B1933+16 was modelled in section 4.4.1 in D17, whereas the PA track bifurcation of B1237+25 was interpreted in section 4.7 therein. Here those interpretations will be modified and will be made consistent with each other.

An interesting example of the core PA distortion is provided by the millisecond pulsar PSR J0437–4715 (Navarro et al. 1997, hereafter NMSKB97, Osłowski et al. 2014). As shown in Fig. 4 (after NMSKB97), at 660 MHz the PA curve steeply dives to the vicinity of orthogonal mode, then immediately retreats in another nearly full OPM jump. The retreat is associated with the sign change of V and a minimum in L/I (which is not quite vanishing). The first quasi-OPM transition, however, is associated with a high level of $|V|/L$. Section 4.4 in D17 describes an effect of symmetric twin minima in L/I which are associated with symmetric profile of V/I . Both these minima have identical look and identical origin. In PSR J0437–4715, however, the observed minima are dissimilar and have clearly different origin. Moreover,

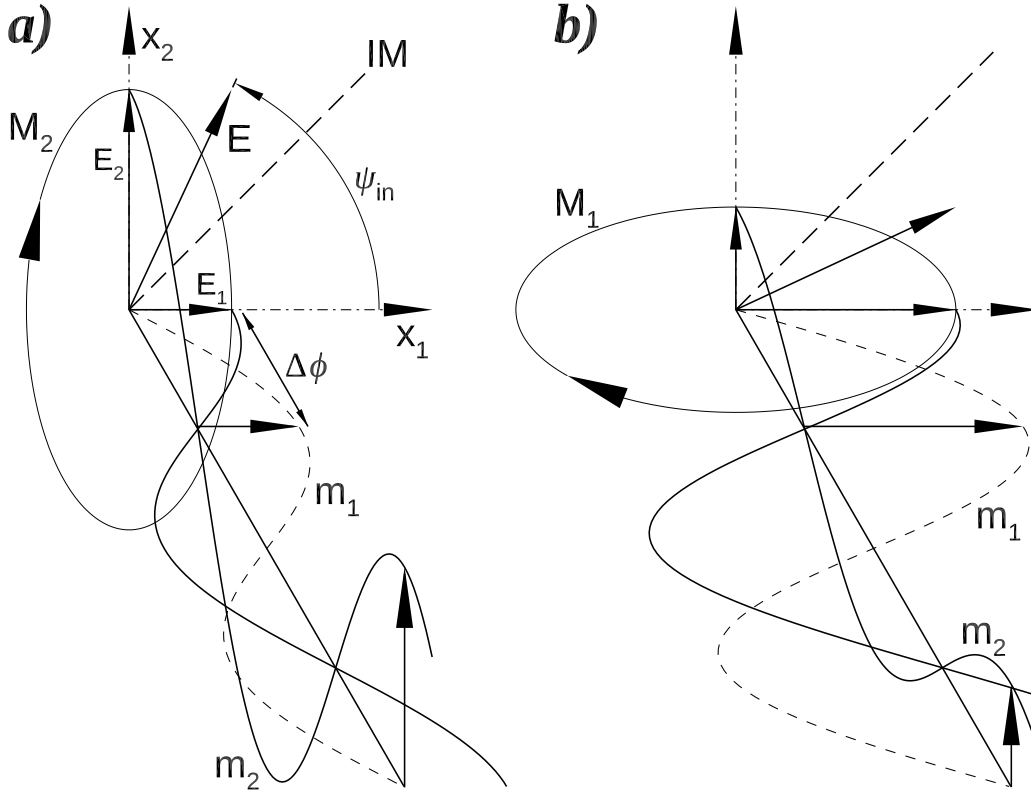


Figure 5. The origin of observed coproper OPMs (represented by the ellipses M_1 and M_2) as the coherent sum of phase-lagged proper mode waves m_1 and m_2 . The linearly polarized proper waves m_1 and m_2 are fed by the linearly polarized wave \vec{E} , which enters a linearly birefringent medium at the mixing angle ψ_{in} . The proper polarization directions of the medium are presented by \vec{x}_1 and \vec{x}_2 , $\Delta\phi$ is the phase lag acquired from refraction index difference, and IM is the intermodal separatrix at $\psi_{in} = 45^\circ$ (the crossing of which corresponds to the pseudomodal OPM transition). The phase lagged position of the proper wave m_1 is shown with the dashed line. For the selected ψ_{in} , the observed OPMs (M_1 and M_2) have the same handedness.

when viewed at different frequencies (NMSKB97) the minima seem to move in longitude at a different rate. They seem to pass across each other which is apparently related to ν -dependent amplitudes of the negative and positive V , and is accompanied by strong changes of PA distortions. Overall, the behaviour of polarization in PSR J0437–4715 looks as a clear manifestation of two independent processes that overlap in pulse longitude.

Another strange polarization effect can be seen on the trailing side of the core component in J0437–4715 (Fig. 4, $\Phi \in (200^\circ, 220^\circ)$). The PA there seems to be freely wandering with no obedience to any RVM-like curve. Off-RVM PA values must also be involved in a phenomenon of non-orthogonal PA tracks, that is often observed in many pulsars (eg. B1944+17 and B2016+28, both at 1.2 GHz in Fig. 15 of MAR15). Apparently, any successful pulsar polarization model must be capable of easily detaching from RVM.

2.2 Modelling hints

The PA loop of B1933+16 has been interpreted in D17 as a sudden rise (and a following drop) of a phase lag between two linearly polarized orthogonal waves, supposedly representing the natural propagation modes. The model is quite successful because it can reproduce all relevant polarization characteristics, such as the nearly bifurcated distortion of

PA, the twin minima in L/I , and the single-sign V with a maximum at the modal transition. Moreover, with a change of a single parameter (amplitude ratio of modes) the model consistently reproduces the change of these features with frequency ν . All this occurs because within the loop, the underlying PA track (which gets split into the loop as soon as the lag is increased) is assumed to be displaced by about 45° from the linear natural modes.

However, the data (see Fig. 1 in MRA16) clearly show that the loop opens on a PA track that can be considered as one of the normal OPMs (as evidenced by a regular OPM jump observed just left to the loop). The model thus requires the modal power to be $\sim 45^\circ$ away from where the power is actually observed to be, if the identification of the observed OPMs as coincident with the normal modes is correct. As described in D17, the observed OPMs are sharp spikes of radiative power with the PA coincident with that of the natural propagation modes. As shown in Fig. 5 the observed orthogonal modes (M_1 and M_2) are produced when the phase lag distribution extends to 90° , since at this value a linearly polarized input signal of any orientation is always decomposed into polarization ellipses aligned with the linearly polarized natural (proper) modes m_1 and m_2 . As emphasized in D17, the observed OPMs (M_1 and M_2) are not the same as the proper modes m_1 and m_2 , because M_1 and M_2 may have the same handedness despite being orthogonal

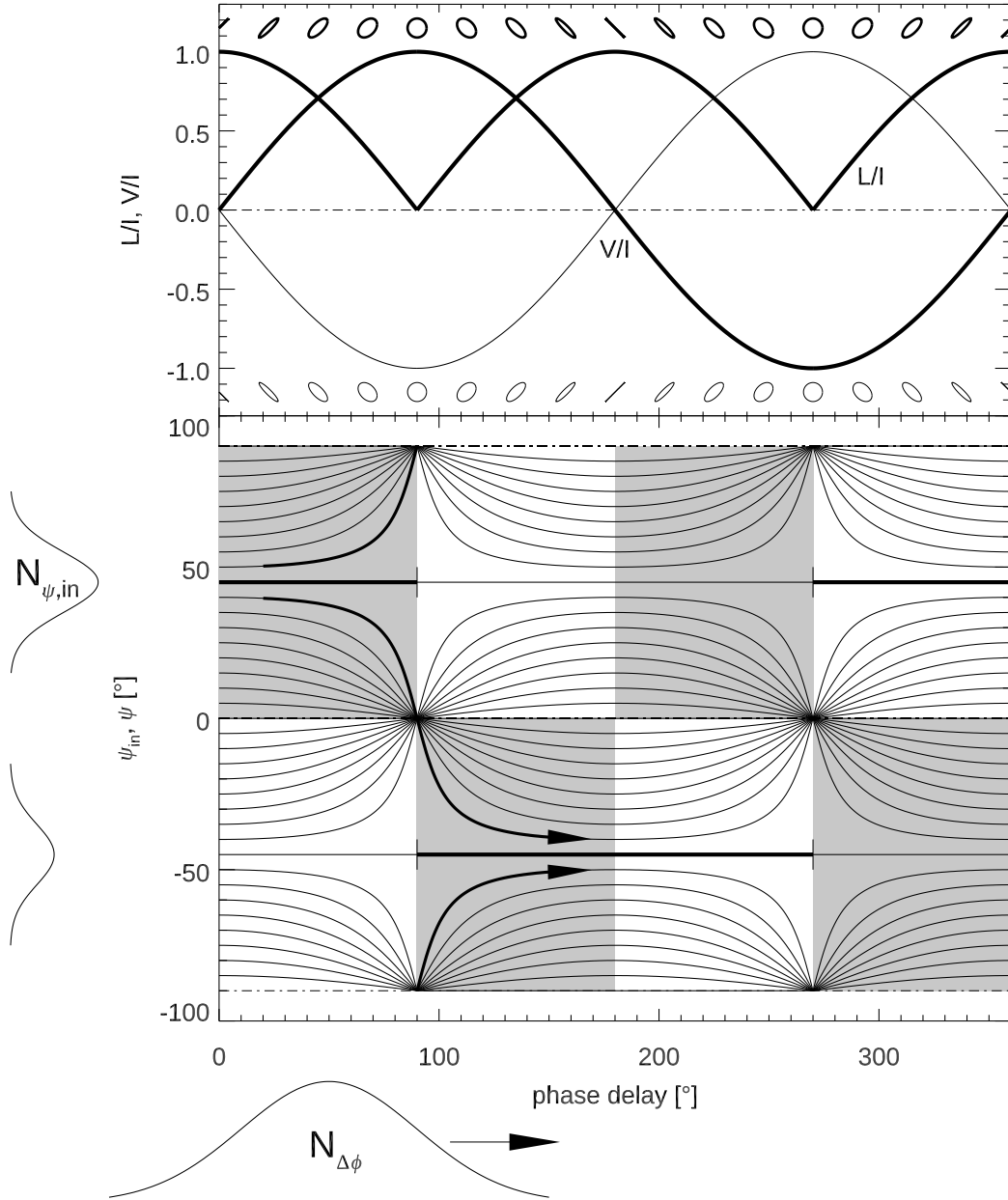


Figure 6. Polarization characteristics of a signal that is a coherent sum of two orthogonal linearly polarized waves. Bottom panel: PA as a function of phase lag. Different curves correspond to a fixed wave amplitude ratio $E_2/E_1 = \tan \psi_{in}$, with the mixing angle ψ_{in} separated by 5° , as shown on the vertical axis ($\psi_{in} = \psi(\Delta\phi = 0)$). The horizontal pieces of straight lines at $\pm 45^\circ$ correspond to polarization ellipses shown in the top panel. Grey rectangles present regions with positive V . The thick arrows diverging from $\psi_{in} \approx 45^\circ$, and converging at $\psi_{in} \approx -45^\circ$ present the phenomenon of the lag-driven PA-track bifurcation. Statistical distributions of lag and mixing angle are shown on the margins. The $N_{\psi, in}$ distribution has two components (at $+45^\circ$ and -45°) which produce opposite circular polarization. Top panel: polarization ellipses and polarized fractions L/I and V/I for the equal amplitude case of $\psi_{in} = +45^\circ$ (thick solid) and -45° (thin). L/I is identical in both cases.

to each other (such case is shown in Fig. 5). However, M_1 and M_2 have the same PA as the proper (normal) waves. Therefore, the linearly-fed observed OPMs M_1 and M_2 will be called below the ‘coproper’ modes.

Because the above-described 45° difference was hard to justify, the analysis that followed in D17 attempted to interpret the core polarization through changes of mode amplitude ratio with pulse longitude (instead of the phase lag). The amplitude ratio was parametrized by the mixing angle

ψ_{in} , i.e. the angle at which the emitted signal was separated into two linearly polarized natural mode waves (Fig. 5a). Because of the partial geometrical symmetry of the problem, slow changes of ψ_{in} with pulse longitude were essentially able to justify the core polarization behaviour of B1237+25, at least for the upper branch of its bifurcated PA track.

However, PSR B1237+25 exhibits two different states of subpulse modulation: the normal state (N) and the core-bright abnormal state (Ab). In the N state the core PA

mostly follows the upper branch of the split PA track, whereas the lower branch is brightest in the Ab state (cf. Figs. 1 and 6 of SRM13). Despite the change of the branch, however, the sign of V remains the same in both cases. In the ψ_{in} -based model of D17 (section 4.7 therein) this was impossible to achieve, because the diverging branches of the bifurcated track were interpreted purely through departure of ψ_{in} from a natural mode in two opposite directions, and the predicted sign of V is different on both sides of the proper mode. This can be seen in the lag-PA diagram of Fig. 6 which presents selected polarization properties of a wave that is a coherent combination of two orthogonal and linearly polarized waves oscillating at a phase lag $\Delta\phi$. The sign of V , as represented by the grey and bright rectangles, is opposite on each side of $\psi_{in} = 0^\circ$ (which corresponds to one natural mode). Moreover, both the loop of B1933+16 and the PA bifurcation of B1237+25 look as phenomena of the same nature, so it is not Ockham-economic to interpret them in different ways (change of phase lag versus change of mixing angle). In the case of the PA loop of B1933+16, the model based on the ψ_{in} only, could reproduce the twin L/I minima, the single-sign V , and the PA distortion, but was incapable to produce the loop-shaped bifurcation itself (see Fig. 11 in D17). The bifurcation, instead, required the change of the lag (Figs. 12 and 13 in D17).

Below I further elaborate the models of D17 in order to explain the mysterious 45° misalignment which allows us to interpret both phenomena within a unified scheme.

3 INTRODUCTORY MODEL

3.1 Coherent addition of linearly polarized waves

Let us start with the model described in D17: before reaching the observer, a radio signal of amplitude E is decomposed into two linearly polarized waves with orthogonal polarization:

$$E_x = E_1 \cos(\omega t), \quad E_y = E_2 \cos(\omega t - \Delta\phi). \quad (1)$$

The waves may be thought to represent the natural propagation modes of a linearly polarizing, birefringent intervening medium. The main (proper) polarization directions of the medium are \vec{x} and \vec{y} . After a phase delay $\Delta\phi$ is built up between the waves, they combine (are added) coherently, which produces the detectable radio signal. The amplitudes of the combining waves are equal to

$$E_1 = E \cos \psi_{in}, \quad E_2 = E \sin \psi_{in}, \quad (2)$$

where ψ_{in} is the mixing angle that parametrizes the amplitudes' ratio:

$$\tan \psi_{in} = E_2/E_1 = R. \quad (3)$$

The Stokes parameters for the resulting wave (i.e. calculated after the phase-lagged components have been added coherently in the vector way) are given by:

$$I = E_1^2 + E_2^2 \quad (4)$$

$$Q = E_1^2 - E_2^2 \quad (5)$$

$$U = 2E_1E_2 \cos(\Delta\phi) \quad (6)$$

$$V = -2E_1E_2 \sin(\Delta\phi) \quad (7)$$

whereas the linear polarization fraction and the resulting PA are:

$$L/I = (Q^2 + U^2)^{1/2}/I \quad (8)$$

$$\psi = 0.5 \arctan(U/Q). \quad (9)$$

To calculate the observed PA, the coherent-origin angle of eq. (9) needs to be added to the external reference value determined by the rotating vector model:

$$\psi_{\text{obs}} = \psi + \psi_{RVM}. \quad (10)$$

Since we focus on coherent effects, only the value of ψ will be discussed below, but it must be remembered that $\psi = 0$ corresponds to $\psi_{\text{obs}} = \psi_{RVM}$, i.e. the RVM PA corresponds to the orientation of the intervening basis vectors (\vec{x}_1 or \vec{x}_2) on the sky.

Diverse pairs of $(\Delta\phi, \psi_{in})$ in such model give the polarization characteristics presented in Fig. 6. Different curves in the lag-PA diagram (bottom panel of Fig. 6) present ψ calculated for different values of ψ_{in} . The value of ψ_{in} is fixed along each line, except from the horizontal lines at $\psi_{in} = \pm 45^\circ$. In this equal-amplitude case the PA jumps discontinuously by 90° , which corresponds to the transition of the polarization ellipse through the circular stage (see the rows of ellipses in the top panel). The grey rectangles (actually squares) represent the regions with positive V . In spite of the impression made by the checkerboard pattern, the sign of V can change only at $\Delta\phi = n180^\circ$, where n is an integer. A change at $\Delta\phi = 90^\circ + n180^\circ$ is impossible, because no lines cross these values of $\Delta\phi$, except at the dark nodes at corners of the grey regions. The nodes appear because for $\Delta\phi = 90^\circ$ any orientation of the incident wave polarization (hence any amplitude ratio R) produces a polarization ellipse aligned with either \vec{x} or \vec{y} direction of the intervening polarization basis (see D17 for more details).

Because of the noisy nature of pulsar radio emission, in the following numerical calculations the values of ψ_{in} and $\Delta\phi$ are drawn from statistical distributions $N_{\psi, in}$ and $N_{\Delta\phi}$ with peak positions ψ_{pk} and $\Delta\phi_{pk}$ and widths $\sigma_{\psi, in}$, $\sigma_{\Delta\phi}$. The intensity is taken as $I = N_{\psi, in}(\psi_{in})N_{\Delta\phi}(\Delta\phi)$. The results presented in sections (3)-(6) are produced with the same numerical code which is described in detail in sections 3.2.1 and 3.2.2 of D17.

3.2 Another pair of orthogonal polarization modes – equal wave amplitudes

Unlike in D17, however, it is assumed in this section that the incident signal can be represented by two circularly polarized waves of opposite handedness.³ For simplicity of interpretation, in this introductory model the detection of these circular waves (C+ and C- in Fig. 7a and b) is assumed to be non-simultaneous (i.e. the signal produced by C+ is not added coherently to the signal produced by C-). Consider the wave electric vector \vec{E}_+ which traces a spiral that projects on the dotted circle C+ in Fig. 7a. In the aforementioned linearly-polarizing birefringent medium, the wave induces the two linearly polarized waves, marked m_1 and m_2 , and

³ As discussed below, such circular waves can be produced by a decomposition of an elliptically polarized wave in medium with circularly polarized natural propagation modes.

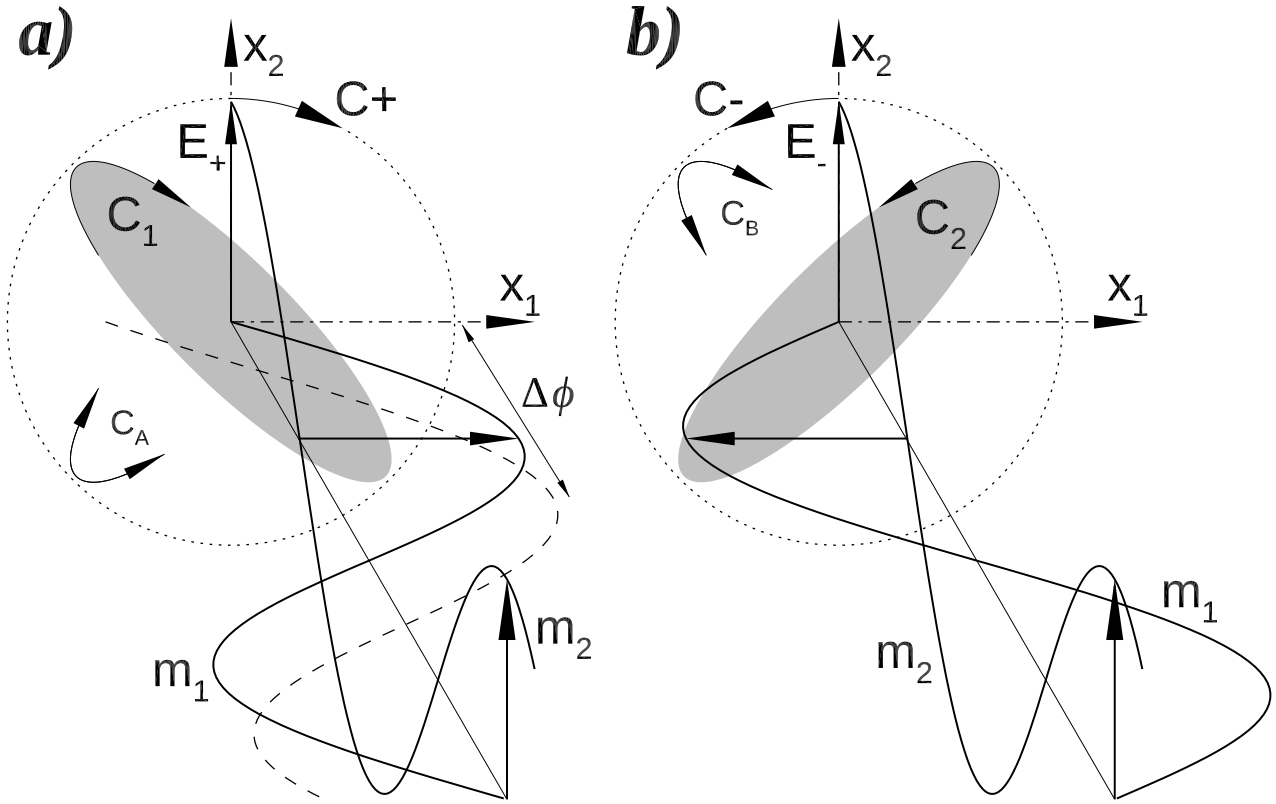


Figure 7. The mechanism of generation of the observed orthogonal polarization modes (grey ellipses C_1 and C_2) in the case of equal amplitudes of the natural mode waves m_1 and m_2 . While the proper mode waves m_1 and m_2 propagate through linearly birefringent medium, they acquire a phase lag $\Delta\phi$ shown on the left. Then they combine coherently into the grey ellipses of the observed OPMs, which are always tilted at $\pm 45^\circ$ with respect to \bar{x}_1 . Larger lags can also produce the pseudomodal ellipses C_A and C_B of any handedness. The proper modal waves are fed by the circularly polarized signals C_+ and C_- , which ensures equal amplitudes of m_1 and m_2 . The circular feeding is not essential for the model if the equal amplitudes are assumed ad hoc, but the origin of the feeding circular waves may be elaborated to justify similar amounts of the observed OPMs C_1 and C_2 (Sect. 5).

described by eq. 1. The original phase delay $\Delta\phi$ between the waves is equal to 90° which results directly from their circular feeding. This phase lag $\Delta\phi$ is assumed to be increased (or decreased) by different refraction indices of the natural propagation modes (therefore, the wave m_1 is shifted to the dashed sinusoid position). Then the modal waves m_1 and m_2 are coherently added, which produces the elliptically polarized observed signal which is presented by the grey ellipse marked C_1 . This is one of the observed OPMs (or one observed PA track, if the name OPMs is to be reserved for the linearly fed coproper OPMs of D17). The eccentricity and handedness of the C_1 ellipse depends on the value of the lag, however, as long as $\Delta\phi$ is between 90 and 270° all the resulting ellipses will have the same PA, precisely at the angle of -45° with respect to the PA of the natural propagation modes.⁴ Larger lags produce another orthogonal ellipse, which is marked C_A in the figure. This second ellipse is 90° away from C_1 and, therefore, may possibly be called the other OPM. However, the C_A mode may have the same handedness as C_1 , so perhaps it should be called a pseu-

⁴ This makes such circular-fed 45° -off modes statistically frequent, which is a feature analogical to the linear-fed modes of D17.

domode.⁵ As explained below, to account for the observed phenomenology, it is necessary to introduce a separate circularly polarized signal of opposite handedness, denoted with C_- and E_- in Fig. 7b. This additional wave, in the same way as just described, produces the second observed OPM, marked with the grey ellipse C_2 . Again, as explained below, the mode may be accompanied by a pseudomode C_B , which may have the same or opposite handedness as C_2 .

Remarkably, the new observed modes C_1 and C_2 form a pair which is 45° away from the natural modes m_1 and m_2 . They are also mid way between the linear-fed modes described in D17, which have the same PA as m_1 and m_2 . The new circular-fed OPMs⁶ can be readily handled with the mathematical model described above, because each observed mode results from coherent addition of phase lagged, linearly polarized orthogonal waves (m_1 and m_2). Specifically, equal amplitudes of the waves imply the mixing angle of $\pm 45^\circ$ (eq. 3) and the circulating feeding of the waves implies the

⁵ Though C_A may have the opposite handedness too.

⁶ The OPMs may also be called same-amplitude OPMs, especially that the circular feeding may be considered irrelevant to the problem as soon as the equal amplitudes are considered as an ad hoc assumption. See, however, Sect. 5.

initial phase lag of $\Delta\phi = 90^\circ$. These are the positions at which the waves E_+ and E_- have to be injected into the lag-PA diagram of Fig. 6. Accordingly, Fig. 8 presents the lag-PA pattern that appears for a single feeding wave (C+) injected at $(\Delta\phi, \psi_{in}) = (90^\circ, 45^\circ)$. Each set of panels in the figure may be considered as presentation of signals detected at a fixed pulse longitude in many different pulse periods. The value of ψ_{in} was sampled from a narrow Gaussian $N_{\psi, in}$ distribution of width $\sigma_{\psi, in} = 3^\circ$ whereas $N_{\Delta\phi}$ had the width $\sigma_{\Delta\phi} = 30^\circ$ (both distributions are shown near the plot axes). The right panels present the distribution of PA angles at a fixed pulse longitude, i.e. they present a vertical cut through those grey-scale PA histograms that are usually shown for single-pulse data (the black thick solid line is the intensity cumulated at a given PA). The distribution of V/I is shown with thick grey line and L/I is thin solid. Fig. 8a shows the case of a one-sided lag distribution, whereas the bottom panels show the symmetric $N_{\Delta\phi}$. Comparison of panels a and b implies that a single circular feed (eg. C+ at $\psi_{in} = 45^\circ$) can produce two orthogonal PA tracks depending on the shape and position of $N_{\Delta\phi}$. The difference of refraction indices favours the one-sided $N_{\Delta\phi}$, and it is also the case which avoids some depolarization typical of the two-sided $N_{\psi, in}$. For the moderately wide lag distribution used in Fig. 8, the power stays close to $\Delta\phi = 90^\circ$ and therefore V/I is high (~ 0.7). L/I is about 0.5 in the top case, and the same in both PA tracks of the bottom-right panel. However, after Stokes-averaging over the PA distribution, the average L/I (at some longitude Φ) would be very low, unlike in the top case. The symmetry of $N_{\Delta\phi}$ distribution is thus important for some conclusions of this paper.

As can be seen in Fig. 8, the lag distribution is extending the grey PA pattern horizontally at $\psi_{in} = \pm 45^\circ$ and it is these horizontal extensions (which can look as dark horizontal bars – see the next figure) that correspond to the observed OPM ellipses C_1 and C_2 in Fig. 7. The more these ‘dark modal bars’ are centered at $\Delta\phi = n180^\circ$, the higher is the local L/I (in a single PA track) and the smaller is $|V/I|$ (this can be deduced from top panel of Fig. 6).

The important general implication of this section is that after statistical averaging over $N_{\Delta\phi}$, the observed OPMs (or the observed PA tracks) have the PA that is *different* from the PA of the natural mode waves m_1 and m_2 (this PA is equal to 0 or 90° , as measured from the \vec{x}_1 axis of Fig. 7). In the specific case considered (equal amplitudes of the natural modes, $\psi_{in} = 45^\circ$), the observed OPMs are located mid way between the natural modes. Thus, *the observed PA tracks are not equivalent to the natural mode waves*. As shown further below (Sect. 7.5), the PA tracks may in general be displaced by an arbitrary, mode-amplitude-ratio-dependent angle (and a ν -dependent angle) from the natural modes. In the special case of equal amplitudes (of the natural mode waves m_1 and m_2) the two observed PA tracks (C_1 and C_2 , or C_1 and C_A) are separated by 90° from each other, and can easily be misidentified as the natural orthogonal modes, although they are misaligned by 45° from the natural modes m_1 and m_2 .

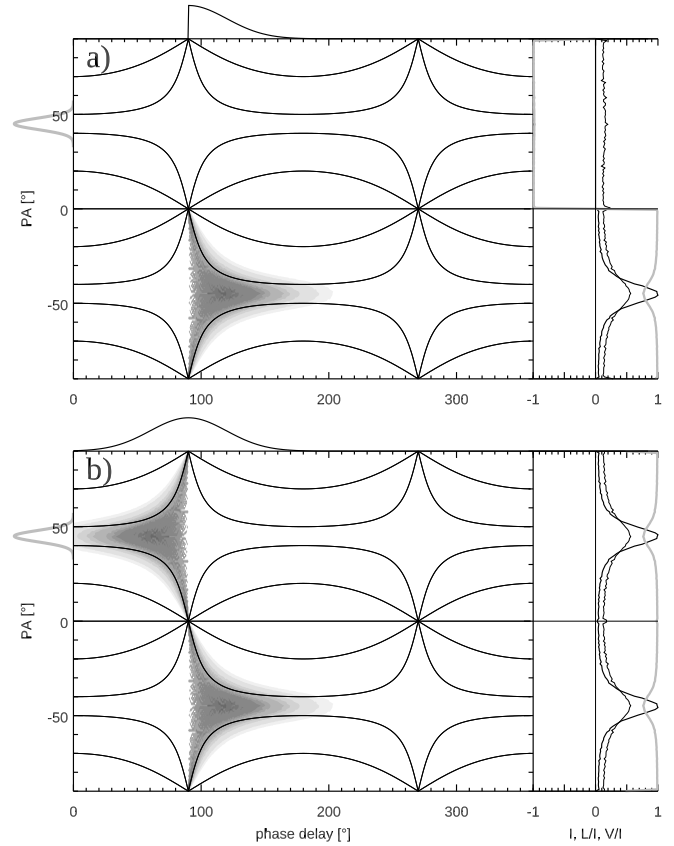


Figure 8. Polarization characteristics for a mixture of non-simultaneous signals, each of which is composed of the coherently added natural modal waves m_1 and m_2 . The phase lag $\Delta\phi$ and mixing angle ψ_{in} for the coherent addition were sampled from the statistical distributions shown near the top and left axes of the plot (in **a** $N_{\Delta\phi}$ is asymmetric). The result can be considered to present distribution of many radio signal samples observed at the same pulse longitude in different pulsar rotations. The main panels present the pattern of observed radiative power on the lag-PA diagram. The right panels present the observed intensity (thick solid), L/I (thin solid), and V/I (light grey) as a function of PA. Thus, the right panels show a vertical cut through the customary plots of PA distributions that are often presented for single pulse data. The result is for $\psi_{in} = 45^\circ$, $\sigma_{\psi, in} = 3^\circ$, $\Delta\phi_{pk} = 90^\circ$ and $\sigma_{\Delta\phi} = 30^\circ$.

4 BASIC PROPERTIES OF THE EQUAL-AMPLITUDE OPMs AND THEIR APPLICATION TO PULSAR PROBLEMS

For the circular origin of the coherently combined waves m_1 and m_2 , the value of ψ_{pk} is fixed and $N_{\psi, in}$ must be narrow. Therefore, we are left with only three different processes that can happen to the radiative power on the lag-PA diagram: 1) the lag distribution may move to larger (or smaller) values; 2) the lag distribution may become wider, and 3) the other orthogonal circular-fed OPM can be added as an additional ψ_{in} distribution at -45° , i.e. the ratio of amplitudes of E_+ and E_- may change.

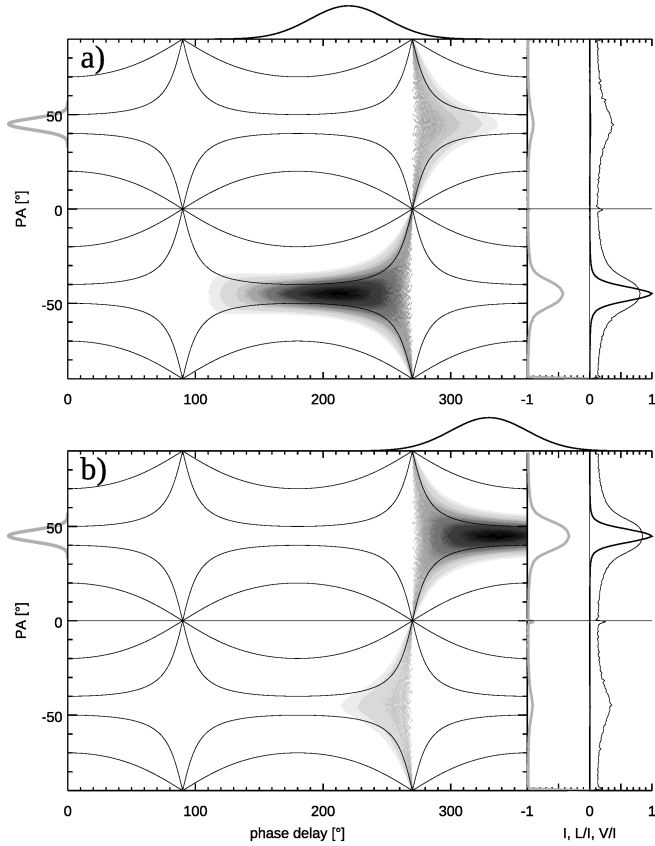


Figure 9. The effect of increasing phase lag $\Delta\phi$. The $N_{\Delta\phi}$ distribution is moving rightward. In **a** $\Delta\phi = 220^\circ$ which causes the sign of V in the bottom PA track to change (compare V in the bottom PA maximum of Fig. 8b), but the PA maximum stays at $\psi_{in} = -45^\circ$. In **b** $\Delta\phi$ increases to 330° which moves the observed PA to $+45^\circ$, but the sign of V does not change. This is called a pseudomodal behaviour. To obtain the normal OPM behavior, another $N_{\psi, in}$ distribution would have to be added at -45° , and the relative power in both $N_{\psi, in}$ would have to change with pulse longitude. The observed modes have the form of dark horizontal bars clearly visible in both lag-PA diagrams.

4.1 Movement of the phase lag distribution

Fig. 9 shows what happens when the phase lag distribution of Fig. 8b moves towards larger values of $\Delta\phi$. In Fig. 9a $N_{\Delta\phi}$ is centered at 220° which is larger than π , hence V of the bottom PA track (at -45°) becomes negative (compare the grey curves in 8b and 9a). The sign of V can thus change within the same PA track. In Fig. 9b the PA track makes an OPM transition to the upper value of $+45^\circ$, however, the circular polarisation stays negative, as in Fig. 9a. Thus, the increase of the lag can cause some OPM transitions, but they do not coincide with the sign change of V . They are actually a quarter of lag-change cycle away, so that the OPM jump occurs at a maximum V , while the sign change of V occurs well within a stable modal PA track, i.e. within flatter parts of a ‘non-transiting’ observed PA track. This is similar to the lag-driven effects in the coproper modes described in D17. The orthogonal modal tracks created by the change of lag (or by widening of $N_{\Delta\phi}$) can thus be called pseudomodes – they do not obey the normal rule of zero V at the minimum L/I . A phenomenon of this type (ie. lag-

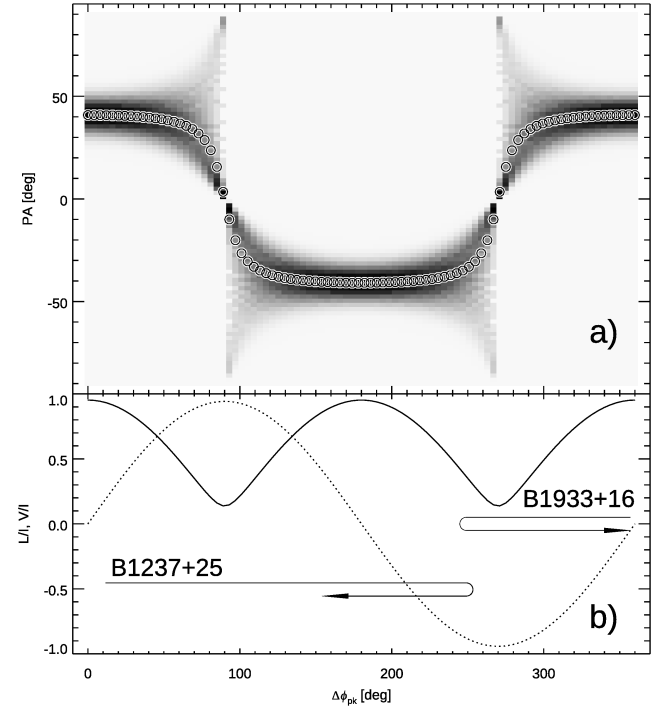


Figure 10. Top: Lag-PA pattern calculated for $\psi_{pk} = 41^\circ$, $\sigma_{\psi, in} = 5^\circ$, $\sigma_{\Delta\phi} = 15^\circ$. Horizontal axis presents $\Delta\phi_{pk}$. Circles show the PA averaged over $N_{\psi, in}$ and $N_{\Delta\phi}$ distributions. The corresponding L/I and V/I is shown in **b**. A change of lag corresponds to the horizontal motion in this plot, as shown with the backward bent arrows. Two interpretations of the core polarization, shown for B1237+25 and B1933+16, work at a single frequency, but fail to explain the frequency behaviour of the phenomenon.

change-based) is observed in several pulsars, eg. in the core PA bifurcations. The lag-driven transfer of power between different OPM tracks also explains the same sign of V in different OPM tracks, as observed in single pulses (MAR15). Superficially similar pseudomodal behaviour is also observed in the form of slow OPM transitions at high $|V|$ that occur within the whole pulse window (eg. in PSR B1913+16, see Fig. 1 in D17, after Everett & Weisberg 2001, also PSR J1900–2600, Johnston & Kerr 2018). However, these are probably caused by the PA wandering which is discussed further below.

The appearance of the equal-amplitude observed modes at the 45° distance from the natural modes is interesting: it *seems* to automatically solve the problem of what the primary observed OPM is doing half way between the natural modes at the entry to the PA loop of B1933+16. It is sufficient to claim that the observed OPMs are 45° away from the natural modes, because their amplitude ratio is close to 1 at this particular frequency. In such case, the PA loop can be explained by a rise and drop of $|\Delta\phi|$, such as marked with the backward-bent arrow in Fig. 10b (right). The resulting loop is shown in Fig. 13 of D17. Such model reproduces several observed properties, such as the bifurcation of the PA track, twin minima in L/I , and the single-sign (negative) V . Moreover, a change of lag within a larger interval, such as shown in Fig. 10b (left) would explain the PA track bifur-

cation of B1237+25, along with the sign-changing V at the core component.

The lag-induced PA bifurcation is also illustrated with the curved arrows in Fig. 6. It can be seen that for the PA track to split, the radiative power must be close to $\psi_{in} = 45^\circ$ (in such case the lines of fixed ψ_{in} diverge up and down from 45°). Both the upward- and downward-heading arrows remain all the time within the grey rectangles of positive V . Thus for the lag-induced PA bifurcation the sign of V stays the same whether the upper or bottom branch of the bifurcation is followed. This would explain why the sign of V is the same in both modulation states in B1237+25: in the bright-core Ab modulation state the lower branch of the bifurcation is followed, but the sign of V does not change (in comparison to the N state).

It is thus found that the lag change is the key factor that affects the PA bifurcations observed both in B1933+16 and B1237+25. Both these phenomena have the same nature, and can be explained by the same model with slightly different parameters. However, the PA loop of B1933+16 may also be interpreted in a different (and better) way, which retains the usual coproper OPMs (with the same PA as the natural waves m_1 and m_2 at 0 and 90°), but assumes a quick change of ψ_{in} towards $\sim 45^\circ$ within the loop. This new interpretation is favoured as discussed later, but such new model also requires the rise and drop of the phase lag within the loop.

The PA bifurcation model that is based purely on the lag-change faces serious problems when the loop of B1933+16 is interpreted at two frequencies. In Sect. 4.4.1 of D17 (cf. Figs. 13 and 14 therein) I have shown that a change of a single parameter – ψ_{in} – from 41° (at 1.5 GHz) to 31° at 4.5 GHz well reproduces the new look of the loop at the higher frequency. This can be inferred from Fig. 6: the curved arrow that follows $\psi_{in} = 40^\circ$ produces the PA amplitude of almost 90° . A similar arrow (not shown) that would follow $\psi_{in} = 30^\circ$ for the same range of lag, would produce a smaller amplitude of PA, consistent with the data at 4.5 GHz (see Fig. 1 in MRA16). The problem is that the change of ν is most naturally associated with the change of phase lag. Even if the mode amplitude ratio (hence ψ_{in}) changes with ν , it is hard to argue that the lag $\Delta\phi$ does not change. For a smaller $\Delta\phi$, the horizontal backward-bending arrow in Fig. 10b (right) would turn back earlier, which would have made the PA amplitude smaller (as observed). However, such earlier backward turn would also cause the twin minima in L/I to approach each other, or even merge into a single minimum at the middle of the loop. This is not observed at 4.5 GHz: the minima in L/I become very shallow but stay at the same Φ (Fig. 1 in MRA16).

Apparently the lag-change alone cannot explain the loop at both frequencies. It will be shown below that simultaneous change of ψ_{in} and $\Delta\phi$ with pulse longitude is needed to understand the phenomenon at both frequencies.

4.2 Changes of width of the lag distribution

Considerable widening of the lag distribution wipes out the circular polarization and tends to produce two highly linearly polarized PA tracks of similar or equal amplitude (which gives zero net L/I at a given Φ). This is because the radiative power is filling in several ‘dark horizontal bars’ at

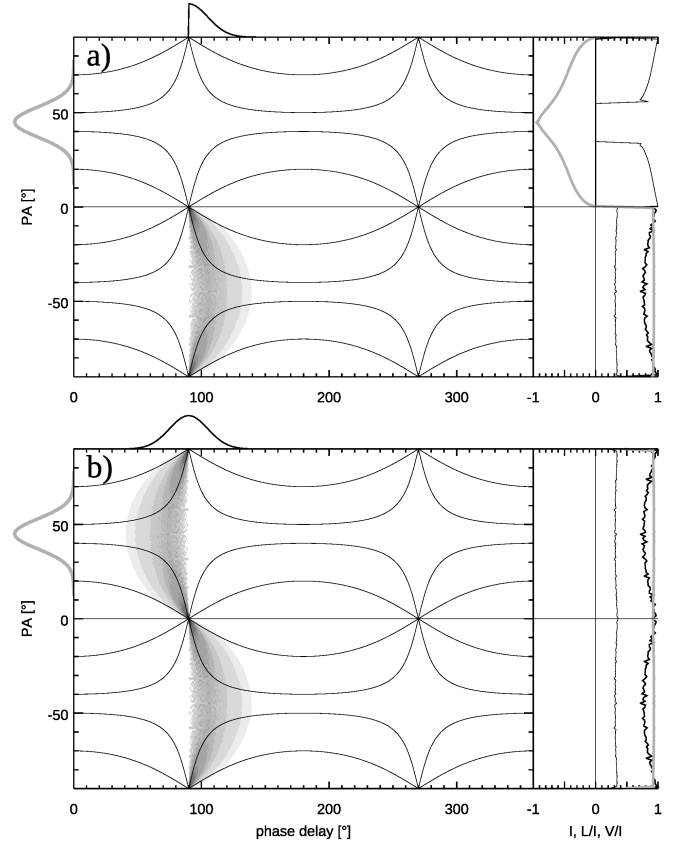


Figure 11. The effect of 45° PA jump, with the associated randomization of PAs visible in the right panels. When $N_{\Delta\phi}$ becomes narrow in comparison to $N_{\psi_{in}}$ the maxima of PA distribution move to 0 and 90° (compare the PA distributions in Fig. 8). The small differences of lag around $\Delta\phi_{pk} = 90^\circ$ result in the randomization of the observed PA, which is similar to the behaviour of B1919+21 at 352 MHz (MRA15).

both 45° and -45° in the lag-PA diagram. On the other hand, for moderately strong widening of $N_{\Delta\phi}$ the results may be similar to those of the $N_{\Delta\phi}$ shift, because the ‘center of weight’ of the widening $N_{\Delta\phi}$ moves rightward.

An interesting effect appears when the lag distribution becomes narrow and has a comparable width to the ψ_{in} distribution ($N_{\psi_{in}}$). Fig. 11 has been calculated for $\sigma_{\psi_{in}} = 8^\circ$ and $\sigma_{\Delta\phi} = 15^\circ$. As can be seen in the right-hand panels, this makes the PA distribution quasi uniform, and the peaks relocate to coincide with the natural propagation modes m_1 and m_2 (located at PA of 0 and $\pm 90^\circ$). The degree to which the peaks stand out depends on the ratio of $\sigma_{\psi_{in}}$ and $\sigma_{\Delta\phi}$, and increases for narrower $N_{\Delta\phi}$. This phenomenon has therefore the key characteristics of the 45° PA jump, namely, the randomization of PA and the appearance of new pair of preferred PA values which are displaced by 45° from the equal-amplitude OPM tracks (observed in the wide- $N_{\Delta\phi}$ case).

The modelled quasi uniform distribution of PA corresponds to the erratic PA spread observed in the central profile region of PSR B1919+21, where the average PA curve is displaced by 45° (see Fig. 18 in MAR15). The chaotic (quasi-uniform in the model) distribution of PA becomes visible because the narrow $N_{\Delta\phi}$ is negligible, so the observed signal directly presents the state with no additional phase lag

between the linear components m_1 and m_2 . In this way the circulating motion of the electric field E_+ , as presented by the dotted circle C+ in Fig. 7a becomes directly visible (the circulation is recovered as the sum of the m_1 and m_2 waves with the little-changed original phase delay of 90°). Surprisingly, then, according to the circular-fed equal-amplitude model, the observed erratic PA spread also has geometric origin: it results from the circulating motion of the incident circularly polarized signal. The observed 45° PA jump thus represents the transition from the lag-spread-stabilized PA (which represents the state of quasi-noncoherent average) to the lag-sensitive chaos of coherent states. In such model, the narrow well defined PA tracks present the observed OPMs (ie. the grey ellipses C_1 and C_2 that are misaligned by 45° from the natural modes) which are associated with an average of wide $N_{\Delta\phi}$ -distribution. The longitudes with the erratic PA, on the other hand, present the non-averaged emission in which case the natural propagation modes m_1 and m_2 get through essentially undelayed. This interpretation, therefore, also associates the observed OPM tracks with the intermodes, just as the aforescribed PA bifurcation model does.

The PA randomization of Fig. 11 has been obtained for a single OPM signal (say, C_1 fed by C+, contributing the $N_{\psi, in}$ distribution at $+45^\circ$ in Fig. 7). In this case the circular polarization can stay larger than zero throughout the 45° jump, as observed in B0823+26 (Everett & Weisberg 2001). The addition of the second orthogonal mode (C_2 or C- in Fig. 7) allows to suppress V arbitrarily strongly.

The phenomenon of the 45° jump was interpreted in D17 as the narrowing of the lag distribution, which is maintained here. However, the orthogonal modes that correspond to the wide $N_{\Delta\phi}$, and are observed at the profile outskirts in B1919+21, were interpreted differently, and the peak of the $N_{\psi, in}$ distribution in the narrow lag state was arbitrarily positioned near $\psi_{in} = 45^\circ$. In the model discussed in this section the nature of the observed OPMs is different (circular fed C_1 and C_2) and they automatically tend to stay at the 45° distance from the orthogonal proper waves (m_1 and m_2).

The widening and displacements of $N_{\Delta\phi}$ produce the pseudomodal behaviour – they are incapable of reproducing the classical mode jumps with coincident minima of L/I and $|V|/I$. To obtain such regular behaviour it is necessary to introduce the second circularly polarized component that produces the C_2 OPM. This rises the question of why the amplitudes of these circular waves tend to be close to each other, and what causes the amplitude ratio to invert at the regular OPM jumps.

5 PULSAR AS A PAIR OF BIREFRINGENT FILTERS

5.1 Similar amount of pulsar OPMs in the circular-fed model

It has been shown above that some pulsar polarization effects can be described as the linearly birefringent filtration of two circularly polarized waves of similar amplitude but opposite handedness. If added coherently, such circular waves combine into a linearly polarized wave, or an elliptically polarized wave with large eccentricity of its polarization ellipse

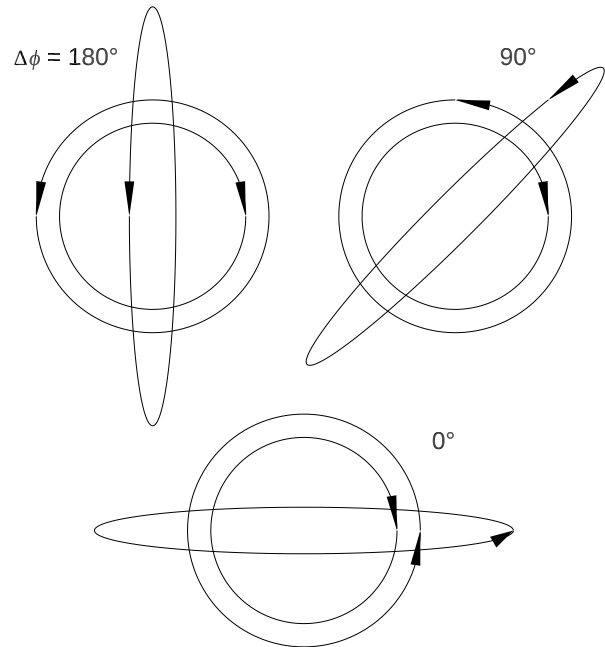


Figure 12. The almost linearly polarized signal, represented by the narrow polarization ellipse, can be mathematically decomposed into circularly polarized waves of similar amplitude. The same decomposition can occur in circularly birefringent medium. Rotation of the quasi-linear signal only changes the oscillation phases of the circular waves (tips of arrows refer to the same moment of time, and numbers give the phase difference). The waves' amplitudes are unaffected (cf. the Faraday rotation effect).

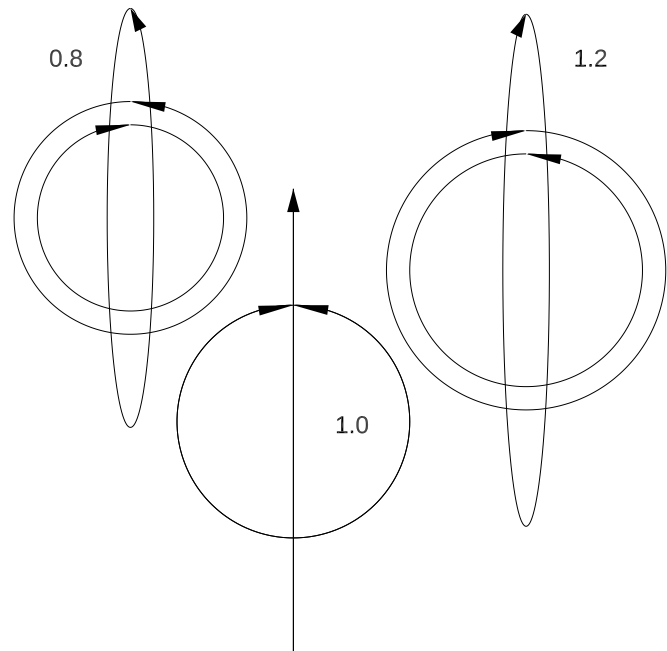


Figure 13. Decomposition of the quasi-linearly polarized signal into circularly polarized waves. The amplitude ratio of the waves (equal to 0.8, 1 and 1.2 in the cases shown) depends on the eccentricity of the signal's polarization ellipse. With the change of handedness, the relative amplitude of the circular waves is inverted.

(see Figs. 12 and 13). This suggests that both these circularly polarized waves (C+ and C-) are generated by a single emitted signal with a narrow polarization ellipse. Such original signal may be split into two circularly-orthogonal waves in medium with circularly polarized natural propagation modes. If the original (i.e. emitted) signal is completely linearly polarized, as in the middle case in Fig. 13, then it produces identical amplitudes of both these circular waves (C+ and C-).

In D17 the circular wave stage of the model was absent. Along with the change of pulse longitude Φ , the electric vector \vec{E} of the emitted linearly polarized signal was slowly rotating with respect to the intervening polarization basis (\vec{x}_1, \vec{x}_2) . The reason was the change of angle between the low- and high-altitude direction of charge trajectories (section 4.5 therein). Whenever the vector \vec{E} was passing through the 45° angle, i.e. mid way between \vec{x}_1 and \vec{x}_2 , the mode amplitude ratio was inverted. This was causing the 90° OPM jumps, albeit of the pseudomodal nature (with $|V|$ peaking at the minimum L/I).

In the present circular-fed model such effect is not possible, because the rotation of the initial linearly polarized (or slightly elliptical) signal does not affect the amplitudes of the circular waves C+ and C-. The rotation just changes the phases of the waves, as shown in Fig. 12 (it is the Faraday rotation effect). Whatever the absolute oscillation phase of the circular waves, they always feed the same, orthogonal and linearly polarized waves m_1 and m_2 . However, the ellipticity and handedness of the initial signal do affect the amplitudes of C+ and C-. As illustrated in Fig. 13, the relative amount of the circular waves is inverted whenever the handedness is changed, and the amplitude ratio is determined by the eccentricity of the initial signal.

Therefore, in the model with the filtration of the initial signal by the circularly-birefringent medium the regular OPM jumps (with the coincident minima of $|V|/I$ and L/I) are caused by the change of handedness of the emitted signal. It is the handedness of the emitted radiation which determines which circle in Fig. 7 is larger, and which $N_{\psi, in}$ distribution – whether the one at 45° or the one at -45° – is stronger, i.e. higher.

5.2 The regular OPM jump in the center of radio pulsar profiles

There is a way to test the hypothesis that the regular modal jumps are caused by the handedness change. It is well known that the regular inversion of the mode amplitude ratio is often observed in the central parts of pulsar profiles. The millisecond pulsar PSR J0437–4715 provides an example of this effect, as evidenced by the sign change of V and OPM jump at the normally behaving L/I minimum (see Fig. 4). Such sign-changing, sinusoid-like profile of V has long been associated with a sightline traverse through a fan beam of curvature radiation, the latter being emitted by a bent stream of charges (e.g. Michel 1991, pp. 355 - 359). The ensuing pulse of curvature radiation, at least in vacuum theory, has precisely the sinusoid-like, handedness-changing profile of V . As a consequence of the geometry shown in Figs. 13 and 7, there should be a regular 90° OPM jump produced by the change of handedness, and it is indeed often

observed at zero V in such core components of supposedly curvature-radiation-related origin.⁷

Thus, pulsar magnetosphere consisting of two filters that are made of circularly and linearly birefringent materials provides a quite successful polarization model: it is capable of explaining both the above-described non-RVM peculiarities and the standard polarization properties such as comparable modal power and the regular OPM jumps. However, such model is complex and difficult to justify physically. A possible physical scenario would include a low altitude emission of the nearly linear signal, followed by the circular decomposition in weak magnetic field at large altitudes. The final stage of the linear filtering could possibly be considered as equivalent to the effects that occur at the polarization limiting radius. Because of this complexity, in what follows the relative amplitude of the opposite- V modes is considered as a free parameter.

6 TWOFOLD NATURE OF PULSAR POLARIZATION

It was shown above that aside from the RVM effect, the polarization of pulsar radio signal can change because of two independent reasons: 1) as a result of change of the lag distribution $N_{\Delta\phi}$ and 2) as a result of change of the modal amplitude ratio (expressed by the ratio $|\vec{E}_+|/|\vec{E}_-|$ in the circular-fed model). The first factor likely depends on the local properties of the intervening matter: a temporary increase of refraction index may appear when the line of sight is traversing through some extra amount of matter, e.g. a plasma stream. The second factor is likely governed by the radio emission process (and is determined by the ellipticity and handedness of the emitted radiation in the specific case of the filter pair model). The two mechanisms – the lag-driven and amplitude-driven changes of polarization – have markedly different properties. The lag-driven effect produces the anticorrelated variations of $|V|/I$ and L/I with pulse longitude (and OPM jumps at maximum $|V|/I$). The amplitude-driven effects generate the regular modal behaviour with the usual OPM jumps.

These generic properties are illustrated in Fig. 14 which presents a regular OPM transition on the left ($\Phi \approx 120^\circ$) and the lag-driven bifurcation of the PA track on the right ($\Phi \approx 290^\circ$) as a function of pulse longitude. The regular OPM coincides with the mode amplitude ratio of 1. The relative power of both modes, hereafter denoted Z , can be expressed as the integrated power (or just height, in case of identical width) of the $N_{\psi, in}$ distribution at $+45^\circ$ and -45° . The increasing value of $Z \times 100$ is shown in the top panel (dotted), along with a temporary increase of $\Delta\phi_{pk}$

⁷ The orthogonal elliptically polarized modes have by definition the opposite handedness, so it may seem to be a trivial vicious circle argument that a change of V sign confirms a modal jump. However, it is not, because without the final linearly birefringent filtering, the circular waves of Fig. 13 would combine back to the original ellipse or would be observed as separate circularly polarized signals. So it is the pair of filters which produces the regular OPM jumps.

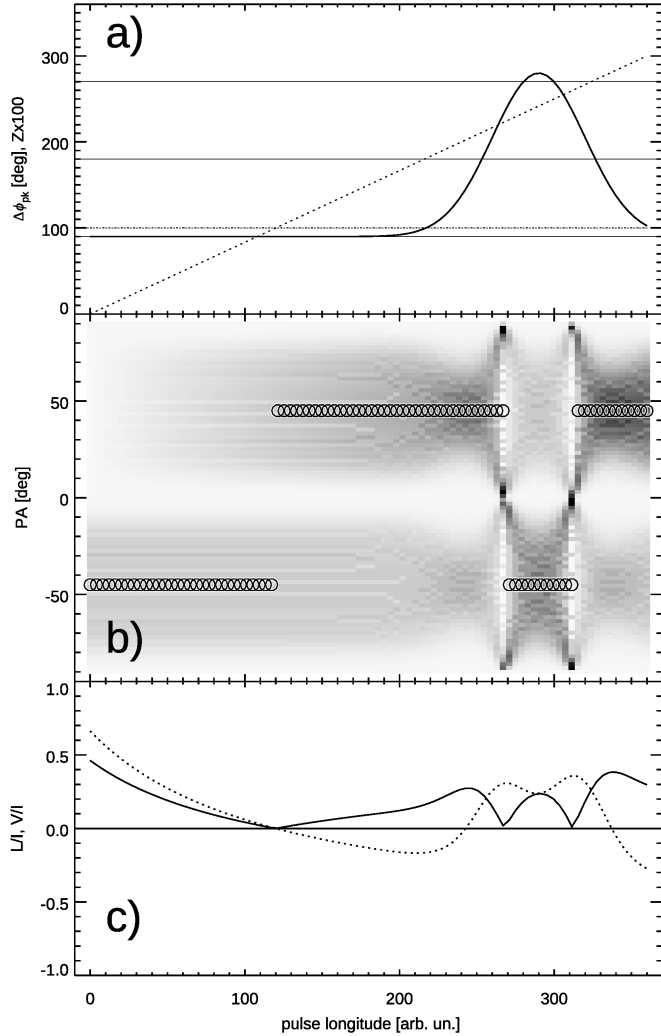


Figure 14. Two generic polarization effects in the coherent wave addition model: the regular OPM jump caused by inversion of mode amplitude ratio (left, at $\Phi \approx 120^\circ$) and the lag-driven PA bifurcation/loop effect (right, at $\Phi \approx 290^\circ$), both shown as functions of pulse longitude. Top: the relative power Z of both modes (dotted diagonal shows $Z \times 100$) and the function $\Delta\phi_{pk}(\Phi)$ which follows the Gaussian centered at $\Phi = 290^\circ$. Beyond the Gaussian $\Delta\phi_{pk}$ is equal to 90° . The profiles of L/I (solid) and V/I (dotted) are shown at the bottom. The lag-profile Gaussian has the 1σ width of 30° , whereas $\sigma_{\psi, in} = 13^\circ$, $\sigma_{\Delta\phi} = 45^\circ$.

(solid Gaussian).⁸ Several polarization effects observed in radio pulsars result from either process, or from a mixture of both. As described in section 2.1, both these non-RVM effects appear to shape the observed polarization especially in the central parts of pulsar profile.

Both these effects may depend on frequency. The influence of the lag may depend on ν because the lag depends on the refraction index, which is likely ν -dependent. As for the amplitude-related effects, they need to be ν -dependent to explain the modal power exchange observed in the D-type pulsars by Young and Rankin (2012). This exchange of

⁸ Here ‘temporary’ means ‘constrained to a narrow interval of pulse longitude’.

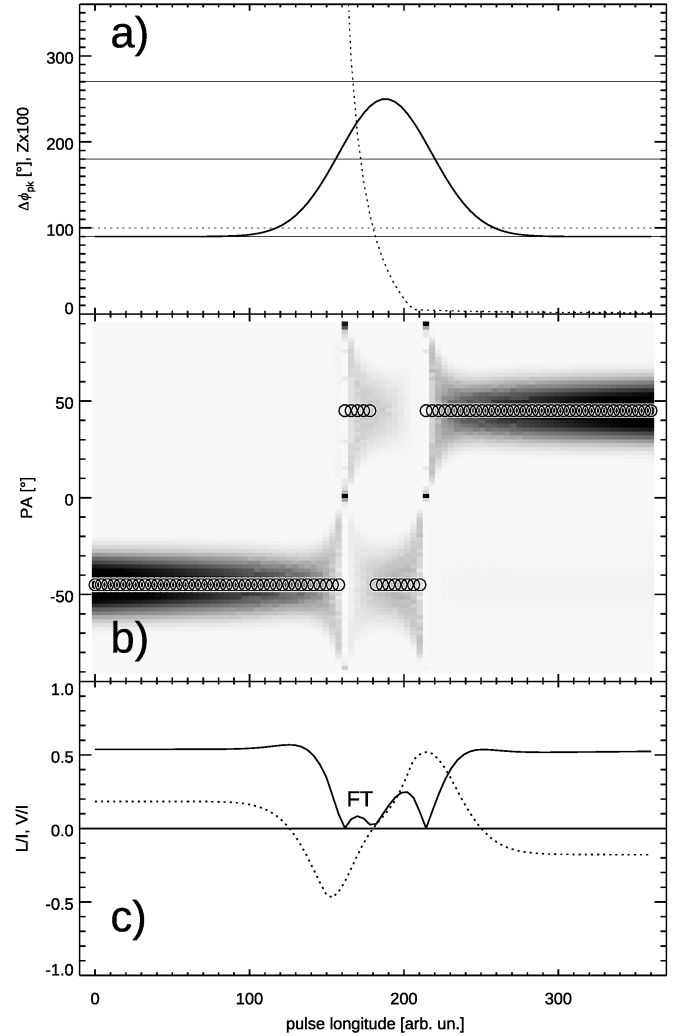


Figure 15. The result of simultaneous operation of both effects – the lag change and amplitude change – within the same longitude interval. Both the $Z = 1$ crossing point and the Gaussian lag-pulse are moved toward the center of the Φ axis. Note the appearance of dissimilar twin minima denoted ‘FT’ that coincide with OPM jumps. The left minimum has high $|V|/I$, the right one coincides with $V = 0$. This is the phenomenon observed in the profile center of J0437–4715. Since Z and the amplitude of the lag pulse depend on ν , the look of this effect strongly depends on frequency. The value of Z is changing as shown with the dotted line in **a**, $\sigma_{\psi, in} = 5^\circ$, $\sigma_{\Delta\phi} = 105^\circ$.

power seems to coincide with the V -sign change, although the radio spectral coverage is far from continuous.⁹ The ν -dependent amplitude ratio is also responsible for another type of PA distortions (slow PA wandering) that is discussed further below.

⁹ In the case of B0301+19, for example, between the 327 MHz and 1.4 GHz Arecibo profiles of Young & Rankin I have only found the 1.22 GHz profile in MRA15. The modal exchange takes place near 1.22 GHz since V has both signs in different parts of the average profile at this ν .

6.1 The origin of dissimilar L/I minima in PSR J0437–4715

While interpreting polarization in the central (or other) parts of any profile it is important to allow for the possibility that both the effects of lag and amplitude ratio may be overlapping there to produce a net profile of L/I , V/I and a net PA. An obvious example of such overlap is the center of the profile of J0437–4715.

Fig. 15 presents model result for the case when the temporary rise of lag (solid line in top panel) roughly coincides in Φ with the amplitude ratio reversal (dotted curve in top panel). The parameters have been changed a bit in comparison to Fig. 14, eg. the rate of Z change was increased, however, the main difference is that the longitude of equal mode power ($Z = 1$) and the peak of $\Delta\phi_{pk}(\Phi)$ profile were displaced to roughly the same Φ . This combination of lag and amplitude effects reproduces the major features of the central profile portion in J0437–4715 at 660 MHz (Fig. 4, after NMSKB97). A double minimum of L/I appears at $\Phi = 170^\circ$ (denoted FT in Fig. 15). The right minimum in this pair coincides with the change of V sign, whereas the left one coincides with high $|V|/I$. The value of L/I in the regular right minimum does not quite reach zero, as in the observation. Within the longitude interval flanked by the minima, the PA is visiting the orthogonal PA track, but quickly returns back to the -45° value.¹⁰ The deep minimum at $\Phi \approx 215^\circ$ does not follow the observations, but this is only because no efforts have been made to adjust parameters in this longitude interval. Another difference is that the modelled OPM follows the full 90° traverse. This is caused by the perfect alignment of the $N_{\psi, in}$ with $\pm 45^\circ$ (this constraint will be relieved below).

The complex polarization of core emission can thus be understood as a combination of the lag-driven and amplitude-ratio-driven polarization effects. The core emission of normal pulsars (eg. B1237+25, B1933+16) also exhibits polarization profiles that are neither symmetric nor antisymmetric. Apparently, the overlap of lag and amplitude effects also occurs in these objects and is partially destroying the anti/symmetry of L/I and V/I which appears when the lag and amplitude phenomena are viewed separately.

6.2 Towards a general model

Let us summarize the results obtained so far. A model based on coherent and quasi-coherent addition of linearly polarized waves of roughly equal amplitude is capable of qualitatively reproducing polarized profiles (ie. all three components: L/I , V/I and PA) of the following phenomena: 1) the bifurcations of PA track in pulsars with complicated core emission (ie. B1933+16 and B1237+25, including two modulation states of the latter) and 2) the mixed core behaviour of J0437–4715. When extended to encompass the origin of the feeding circular waves, the model can possibly justify the regular OPM jumps and the similar amount of modes.

On the other hand, the purely linear birefringent filtering may seem unphysical, and the model faces two problems

that contain indications about how to change it. First, the pseudomodal OPM transitions tend to traverse regions of very low L/I . As can be seen in Fig. 6, for $\Delta\phi$ increasing from zero at $\psi_{in} \sim 45^\circ$ the radiative power approaches the fully circularly polarized point at $(\Delta\phi, \psi_{in}) = (90^\circ, 45^\circ)$ then jumps down to $\psi = -45^\circ$ while staying all the time fully circularly polarized. This is consistent with the low L/I observed at the core PA bifurcations in PSR B1933+16 and B1237+25, however, a capability to flexibly adjust the modelled L/I is needed: in the D17's ψ_{in} -based model of B1913+16 it was difficult to avoid the strong decrease of L/I at the OPM transitions (cf. Figs. 1b and 7b in D17). Second, with the circular feeding of the linear proper waves (m_1 and m_2), the $N_{\psi, in}$ distribution is absolutely tied to $\pm 45^\circ$. Actually, even the spread of $N_{\psi, in}$ around these values (parametrized by $\sigma_{\psi, in}$) is hard to explain.¹¹

The circularly polarized waves (C+ and C-) that feed m_1 and m_2 are then too restrictive for the model and, at least when the ‘filter pair’ concept is dismissed, they indeed do little more than set the equal amplitude ratio of m_1 and m_2 . Therefore, in the following I will use the lone pair of standard, elliptically polarized, orthogonal natural mode waves (EPONM waves). Obviously, the coherent addition of such waves *must* produce all the successful results of previous sections, because the linearly polarized equal amplitude waves are just a special case of EPONM waves. However, the arbitrary amplitude ratio and the nonzero ellipticity provide important enlargement of the model capabilities.

A general model of pulsar polarization thus includes the eccentricity of the polarization ellipse for modal waves (m_1 and m_2). The eccentricity parameter may need to be sampled from statistical distribution of some width. Even with the same eccentricity for both modal waves, this means two new parameters. Along with the other four (the mixing angle for the amplitude ratio and the phase lag, plus the widths of their distributions), this makes up for six parameters. Such parameter space deserves a separate study, therefore, in what follows I describe my calculation method and only present a glimpse of the parameter space – just to address the above-described problems.

7 GENERAL MODEL

7.1 Coherent addition of elliptically-polarized orthogonal waves

The model is conceptually simple: observed pulsar polarization results from coherent and quasi-coherent addition of phase-lagged waves in two elliptically polarized natural propagation modes. They are numbered 1 and 2 and are presented in Fig. 16 by the ellipses m_1 and m_2 . These ellipses are traced by the corresponding electric field waves \vec{E}_1 and \vec{E}_2 . The ellipses m_1 and m_2 should not be mistaken for the observed PA tracks, because the latter result from coherent addition of m_1 and m_2 and may be easily displaced from the natural modes by an arbitrary angle. For example, if equal amplitudes of m_1 and m_2 are preferred, then the observed polarization ellipses (similar to the grey ellipses of

¹⁰ Since the model $N_{\psi, in}$ is perfectly aligned with 45° , one is free to choose whether the PA jump direction is up or down.

¹¹ The displacement from $\psi_{in} = 45^\circ$ could be obtained for elliptically polarized feeding waves.

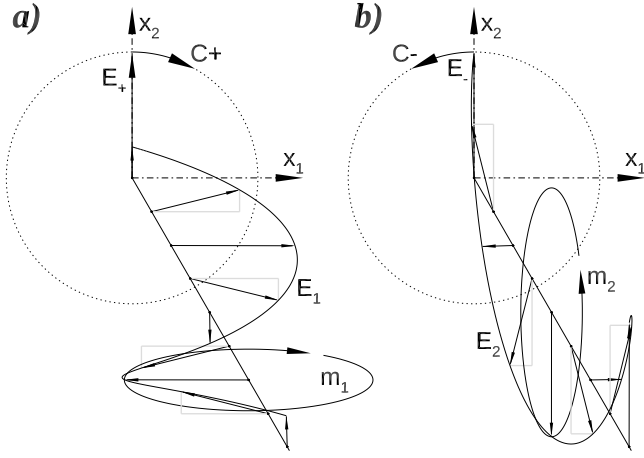


Figure 16. General model of pulsar polarization is based on coherent addition of elliptically polarized natural mode waves E_1 and E_2 which trace the solid line ellipses m_1 and m_2 (shown in **a** and **b**). Here the proper modal waves are fed by the circular waves E_+ and E_- (see Sect. 5), but this is not necessary for the model to work.

Fig. 6) appear at the PA of 45° when m_1 and m_2 are coherently added. The elliptical natural mode waves m_1 and m_2 can be written as:

$$E_1^x = \cos \psi_{in} \cos \beta \cos(\omega t) \quad (11)$$

$$E_1^y = \cos \psi_{in} \sin \beta \sin(\omega t) \quad (12)$$

$$E_2^x = \sin \psi_{in} \sin \beta \sin(\omega t + \Delta\phi) \quad (13)$$

$$E_2^y = \sin \psi_{in} \cos \beta \cos(\omega t + \Delta\phi) \quad (14)$$

where $\Delta\phi$ is the phase delay and $\tan \beta$ represents the ratio of the minor to major axis of the polarization ellipse. As usual ψ_{in} represents the ratio of the modal waves' amplitudes, ie. $\tan \psi_{in} = E_2/E_1$, where $E_1^2 = (E_1^x)^2 + (E_1^y)^2$ and $E_2^2 = (E_2^x)^2 + (E_2^y)^2$. These waves coherently combine into the observed signal that in general is elliptically polarized:

$$E^x = E_1^x + E_2^x \quad (15)$$

$$E^y = E_1^y + E_2^y \quad (16)$$

The polarization ellipse for the observed signal $\vec{E} = (E^x, E^y)$ is calculated by numerically increasing ωt in the range between 0 and 360° . The minor half axis A_{\min} and the major half axis A_{\max} of the observed ellipse are then identified numerically, along with the sense of the electric vector circulation (handedness). The PA is determined by the normalized components of the major axis:

$$\cos \psi = A_{\max}^y/A_{\max}, \quad \sin \psi = A_{\max}^x/A_{\max}, \quad (17)$$

whereas the ellipse axes length ratio gives the observed eccentricity angle:

$$\tan \beta_t = A_{\min}/A_{\max} \quad (18)$$

which is different than the initial β of the proper modal waves. The normalized Stokes parameters are calculated from:

$$Q/I = \cos(2\beta_t) \cos(2\psi) \quad (19)$$

$$U/I = \cos(2\beta_t) \sin(2\psi) \quad (20)$$

$$V/I = \sin(2\beta_t), \quad (21)$$

and the linear polarization fraction is calculated as $L/I = [(Q/I)^2 + (U/I)^2]^{0.5}$.

7.2 Lag-PA diagrams for elliptical modes

The lag-PA diagram of Fig. 17 (left panel) presents the pattern of PA calculated for fixed values of eccentricity β increasing uniformly from 0 to 180° in step of 5° . The amplitudes of the combined modes are everywhere the same ($\psi_{in} = 45^\circ$). The corresponding L/I is shown in Fig. 18, with L/I increasing in darker regions. The sign of V/I is changed several times in the same points of this diagram and, therefore, V/I is not shown. However, $|V/I|$ is as before anticorrelated with L/I , so dark regions in Fig. 18 present low $|V/I|$.

The pattern presents new nodes, ie. regions where there is high probability to observe the radiative flux. The nodes are at $(\Delta\phi, \psi) = (0, 45^\circ)$ and $(180^\circ, -45^\circ)$. They appear for two reasons. The first is that for any eccentricity, at $\Delta\phi = n180^\circ$ the electric vectors of the equal-amplitude modal waves always combine at the PA that is 45° away from the PA of the proper modes (m_1 and m_2 have the PA of 0 and 90°). The second reason is that for the purely linear polarization (infinite eccentricity) of equal-amplitude waves the resulting PA is equal to $\pm 45^\circ$ regardless of $\Delta\phi$. This produces the discontinuous PA jumps between the fixed PA values at $\Delta\phi = 90^\circ$ and 270° . For high eccentricity (nearly linear modal waves m_1 and m_2), and always for equal amplitude, the PA tends to linger close to 45° , which increases the probability of the nearly intermodal PA. This is illustrated in Fig. 28 of the appendix.

The model described earlier in this paper (with the equal-amplitude linearly polarized orthogonal waves, LPOW) was confined only to the horizontal PA segments centered at the new nodes (and some nearby regions because $N_{\psi, in}$ was allowed to have finite width). The lag-PA space of the LPOW model is just a subpart of the new lag-PA diagram and this is because diverse ellipticities are added in Fig. 17. The patterns of L/I and V/I , within the overlapping part of the parameter space, are identical to the one of the LPOW model. For example, the value of L/I in Fig. 18 increases towards $\Delta\phi = n180^\circ$ and decreases at the discontinuous lag-change-driven OPM jumps. The new nodes coincide with the 'dark modal bars' of the LPOW model. This implies that all data interpretations provided before are also possible in the new elliptical model. In other words, the added diversity of eccentricities does not corrupt the previous results.

When the PA values of the left panel are collected in bins on the vertical axis, the histogram shown on the right is produced. The enhancements of the observed OPMs remain at the intermodal positions (half way between the PA of the natural modes). Naturally, for $\psi_{in} = 45^\circ$ ($R = 1$) the intermodal nature of OPMs persists in the presence of diverse ellipticity.

A new feature of the lag-PA diagram are diagonal straight lines which connect the nodes. These correspond to the sum of two circular waves ($\beta = 45^\circ$) at increasing lag. The result is a uniformly rotating linearly polarized signal, hence the linear change of PA (the diagonals thus represent the Faraday rotation effect). A similar case is shown in

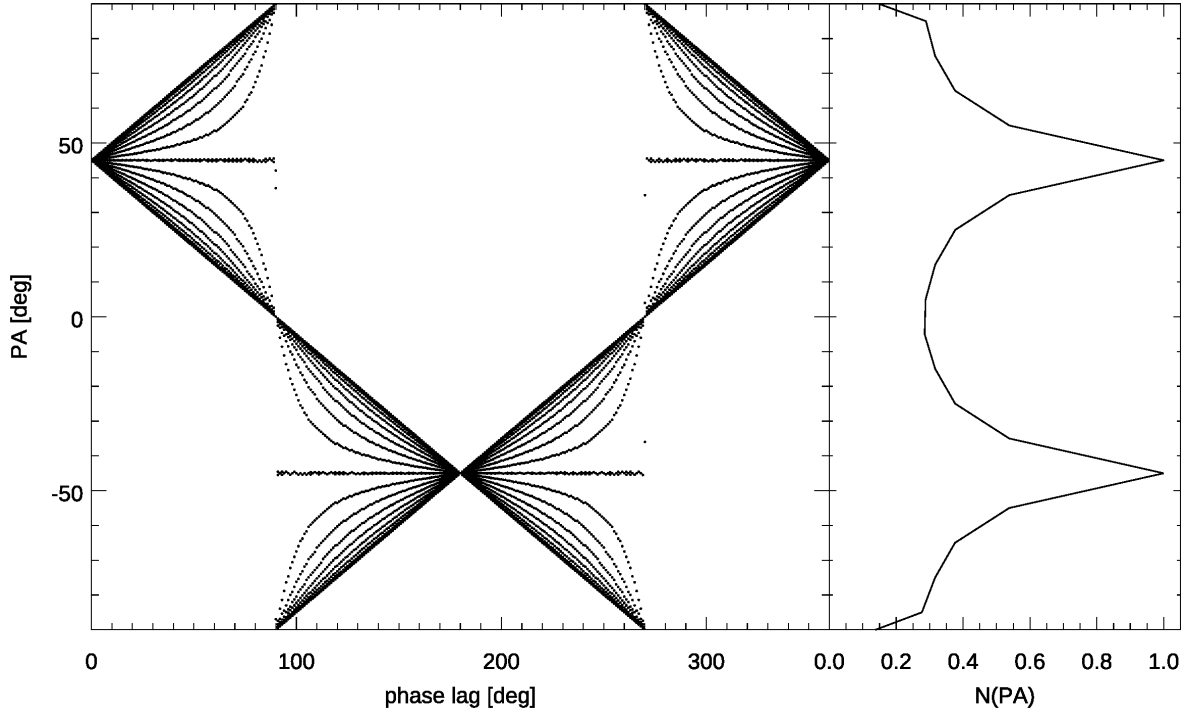


Figure 17. Left: Lag-PA diagram for equal mode amplitudes ($\psi_{in} = 45^\circ$) and for a set of eccentricity parameter $\beta \in (0, 180^\circ)$ sampled at interval of 5° . The horizontal sections ($\beta = 0$, and 90°) are produced by the linearly polarized proper modes as described earlier in this paper. The diagonals correspond to circularly polarized m_1 and m_2 modes ($\beta = 45^\circ$ and 135°) and are caused by the uniform PA change of the resulting fully linearly polarized signal (close cases are shown in Figs. 13 and 29). There are new nodes at $\Delta\phi = n180^\circ$ that coincide with the ‘dark modal bars’ of the previous analysis. Projection of all the PA angles on the vertical axis gives the histogram shown on the right side. The observed OPMs for such equal-amplitude mixture of eccentricities are misaligned by 45° from the natural modes.

Fig. 12 and Fig. 29 in the appendix. The linear polarization is full along the diagonals ($L/I = 1$, $V/I = 0$).

If the radiation at a given pulse longitude contains a mixture of eccentricities, then the lag-driven OPM transition occurs both along the S-shaped (or discontinuous) paths in the lag-PA diagram and along the straight diagonals. As shown in Fig. 18, in the middle of the OPM jump the combining signals of high eccentricity (ie. the almost linearly polarized modal waves which follow the S-shaped path) contribute circularly polarized power (note the bright stripe of the high $|V|/I$ at the position indicated by the arrow) whereas the low-eccentricity signals (circularly polarized modal waves that follow the diagonals) contribute linearly polarized power (the diagonals are black everywhere, ie. they have $L/I = 1$, see Fig. 29, compare Fig. 28). The lag-driven OPM transition for a signal of mixed ellipticity, can thus be perceived as the passage from, say, the top horizontal row in Figs. 29 and 28, to the fourth row in these figures (along with all unshown cases of intermediate ellipticity). As shown in Fig. 18 with the arrow, the inclusion of wider ellipses increases L/I at the lag-driven OPM jump. The inclusion of eccentricity can thus increase the very low L/I at some lag-driven OPM transitions.

7.3 Entanglement of the lag-driven and amplitude-ratio-driven effects

The amplitude ratio of observed OPMs seems to change with pulse longitude Φ and with the frequency ν . The lag change should be considered as the primary effect which governs different look of PA tracks at different ν . The change of mode ratio (or ψ_{in}) is naturally responsible for changes of polarization with Φ (as proved by the regular OPM jumps). However, several observations at different ν suggest that ψ_{in} may also be ν -dependent. Moreover, if some observed OPMs have the intermodal nature, as illustrated in Fig. 7, then it is the change of lag itself, which causes the ratio of observed OPMs to change. This has been presented in Fig. 9, where the change of lag causes the radiative power to leak from one orthogonal PA track to another. It should be possible to recognize if the observed change of OPM amount has the lag-driven origin, because the lag-driven effects exhibit the pseudomodal behaviour (anticorellation of L/I and $|V|/I$). This complexity needs to be kept in mind when the non-equal mode amplitudes are considered.

7.4 Beyond the equal amplitudes

To move $N_{\psi, in}$ away from 45° , the amplitude ratio of the natural mode waves (m_1 and m_2) must be changed to a less

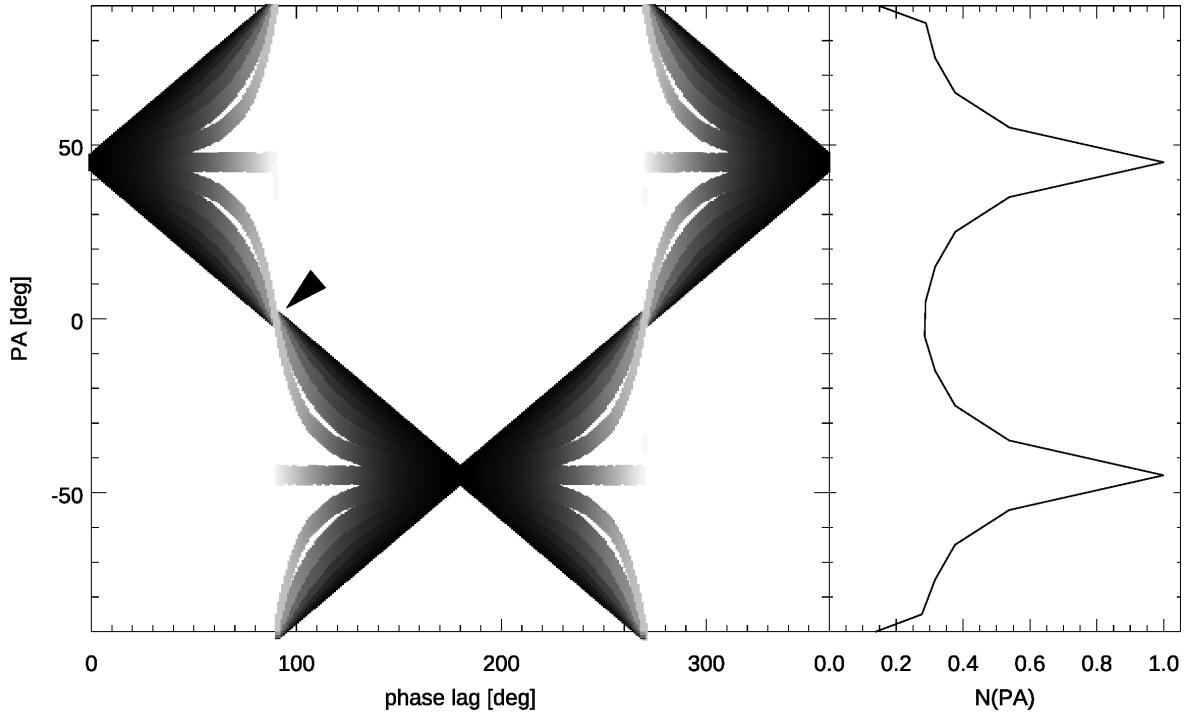


Figure 18. Linear polarization fraction L/I for the lag-PA diagram shown in the previous figure. In the black regions $L/I = 1$, whereas in the bright regions $L/I = 0$. At the point indicated by the arrow several cases of eccentricity overlap, contributing different L/I . The linear (or quasi-linear) modes ($\beta = 0$) contribute circular polarization ($L/I \sim 0$) whereas the diagonals contribute linearly polarized signal ($L/I = 1$). The pattern may also be considered to present $|V|/I$, with the value of 1 in the bright regions, but V/I changes sign several times in a given position of the plot and would require a different type of visualization.

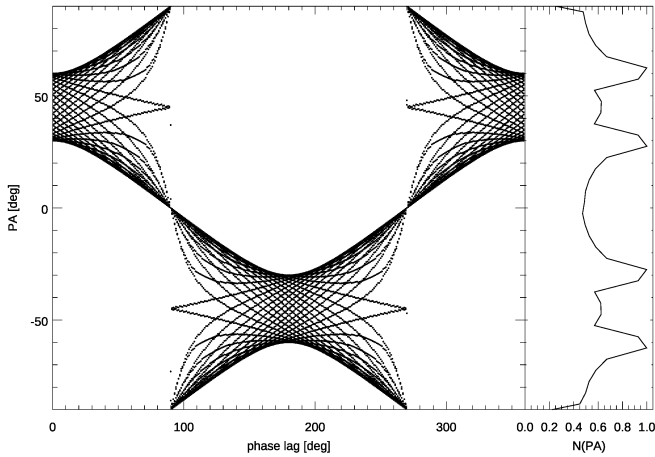


Figure 19. The lag PA diagram for mode amplitude ratio of 0.58 ($\psi_{in} = 30^\circ$). In comparison to the equal amplitude case, the curves of $\psi(\phi)$ have different shape and are displaced vertically. There is a spread of available PA values near the nodes. Note the appearance of the non-orthogonal PA tracks in the histogram. Not all peaks must be observed, depending on the actual spread of β in the observed signal.

trivial value than 1.¹² The change of ψ_{in} causes the entire

¹² To detach from 45° in the circular-fed equal-amplitude model, it is necessary to consider simultaneous detection (and coherent combination) of the modes C_1 and C_2 .

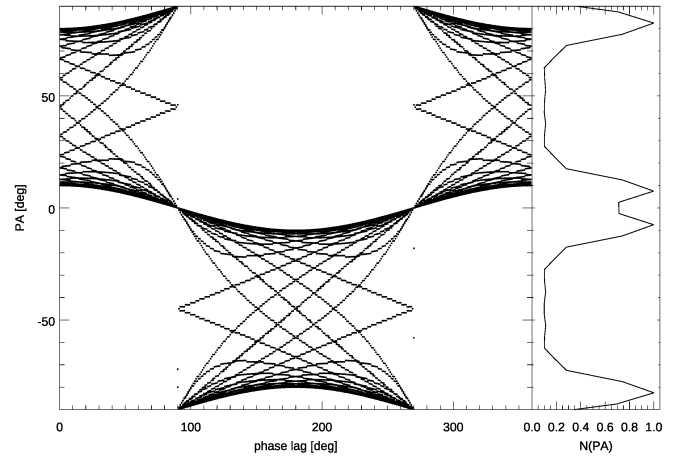


Figure 20. The lag-PA diagram for mode amplitude ratio of 0.18 ($\psi_{in} = 10^\circ$).

lag-PA pattern to evolve. Fig. 19 shows the case of $\psi_{in} = 30^\circ$ (amplitude ratio of 0.58) whereas Fig. 20 is for $\psi_{in} = 10^\circ$ (ratio 0.17). As can be seen in Fig. 19, with the change of mode amount ratio the PA paths move away from 45° . Moreover, with the increase of lag many paths cover smaller range of PA than in the equal amplitude case.

It should be noted that the addition of EPONM waves itself does not imply any preference for the same or similar amount of modes. The intermodal observed OPMs (located at $\pm 45^\circ$, see the histogram in Fig. 17) are just the conse-

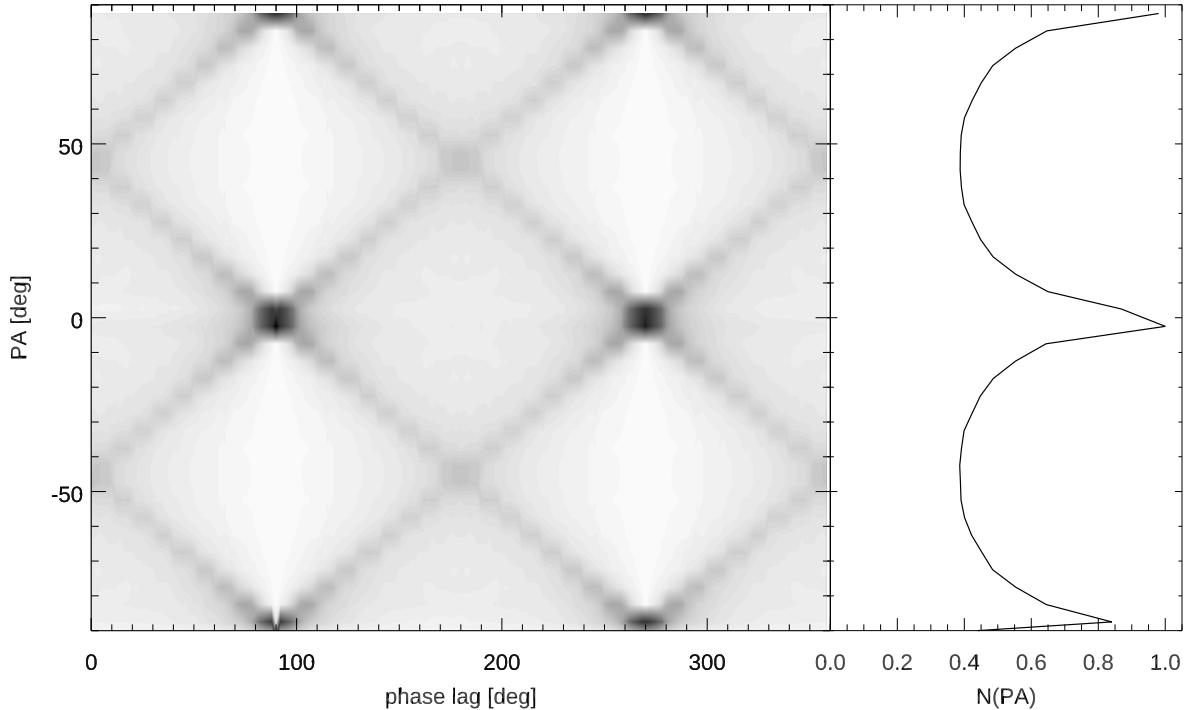


Figure 21. The lag-PA pattern for densely sampled parameter space of $(\Delta\phi, \psi_{in}, \beta)$. The sampling was uniform in all these three angles. The observed PA tracks (peaks in the right histogram) coincide with the PA of the proper mode waves m_1 and m_2 . The black spots at the diagonals' crossings are at the same locations as the linear-fed nodes described in D17 (also see Fig. 6 in this paper).

quence of the equal amplitude assumption. When the entire parameter space is sampled uniformly in $\psi_{in} \in (0, 180^\circ)$, $\beta \in (0, 180^\circ)$ and $\Delta\phi \in (0, 360^\circ)$, the coproper modes of D17 (with the same PA as the natural modes, see Fig. 5) become statistically most probable and stand out in the histogram (see Fig. 21).

In the case of the linear-fed coproper modes (Fig. 5), the equal amplitudes of observed OPMs are produced when the incident linear signal is traversing through the intermodal separatrix IM (at a wide $N_{\Delta\phi}$ that extends to $\Delta\phi = 90^\circ$). This seems to be a quite simple and natural way to change the PA by 90° , but the sign of V does not change along with the PA jump. In the birefringent filter pair model, the equal/similar amplitudes of both opposite- V modes are produced by decomposition of the initial quasi-linearly polarized signal in the circularly polarizing medium of the first filter. Apparently, some mechanism akin to such process is required to explain the nearly equal amount of the modes m_1 and m_2 which are shown in Fig. 16. In any case, if there is any reason for which the natural mode amplitudes tend to be similar, then the histogram of Fig. 17 tells us that the observed OPMs are actually 45° away from the natural propagation modes (as illustrated in Figs. 7 and 28). The dotted circles in Fig. 16 present how the similar amplitudes of modes can be produced if they are fed by the circularly-polarized waves of common origin (ie. produced by decomposition of an almost linearly polarized signal into the C+ and C- waves of nearly equal amplitude).

Finally, however, it must be admitted that amounts of the opposite- V modes are equally often observed to be strongly nonequal. This option opens the possibility to understand the off-RVM wandering of PA tracks.

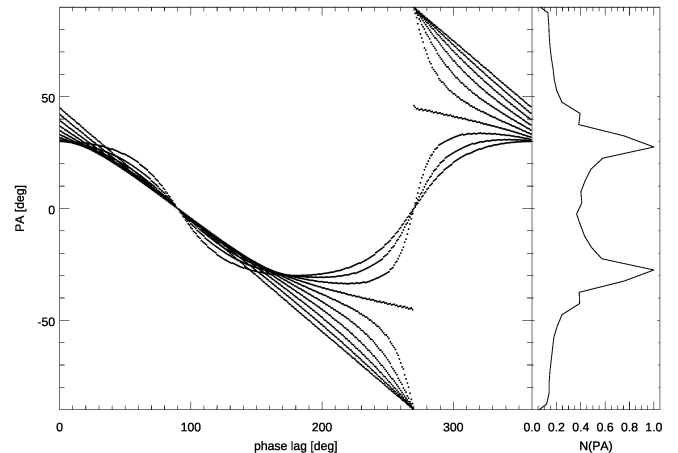


Figure 22. The lag-PA diagram for mode amplitude ratio of 0.58 ($\psi_{in} = 30^\circ$), but with β limited to the interval $(0, 45^\circ)$. The resulting PAs are a subset of those in Fig. 19. Two non-orthogonal PA tracks (visible as the peaks in the right histogram) appear at $\pm 30^\circ$. Changes of ψ_{in} would change the separation between the tracks.

7.5 Mode-intermode PA transitions and the origin of the off-RVM wandering of PA

7.5.1 Non-orthogonal PA tracks

The primary mode exchange phenomenon, illustrated in figures of Young & Rankin (2012) and other observations clearly show that the mode amount ratio changes with frequency. The ratio Z (or R) also changes with pulse longi-

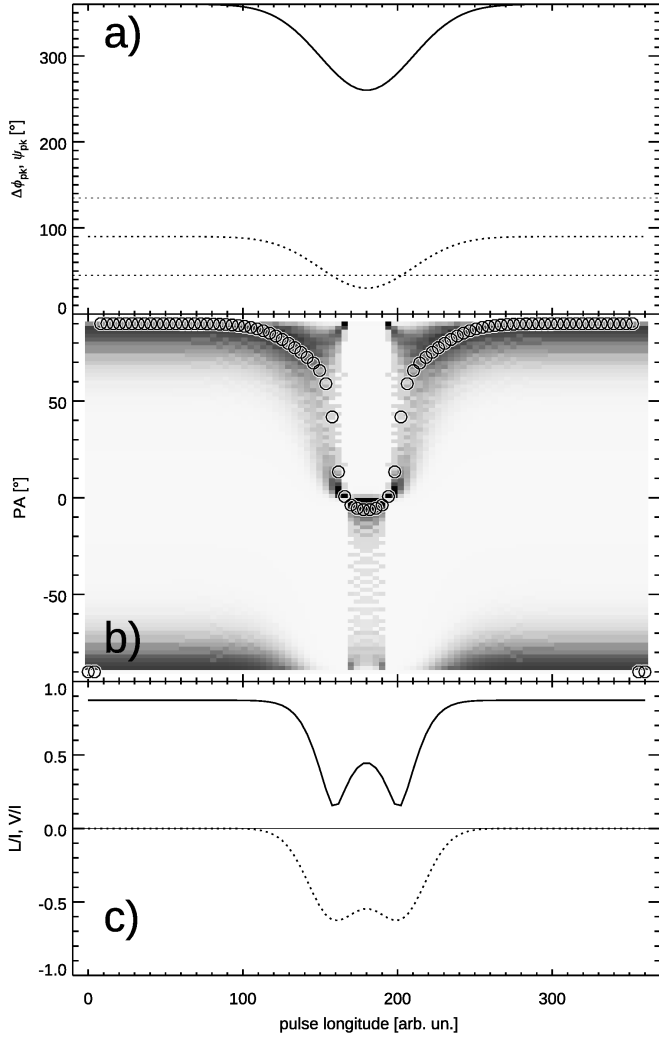


Figure 23. Modelled polarization characteristics for the PA loop of B1933+16 as observed at 1.5 GHz (cf. Fig 1 in MRA16). The loop shaped bifurcation of PA results from the Gaussian variations of ψ_{pk} and $\Delta\phi_{pk}$ (dotted and solid line in a). Distribution widths were kept constant across the feature: $\sigma_{\psi, in} = 15^\circ$, $\sigma_{\Delta\phi} = 45^\circ$.

tude Φ as proved by the regular OPM jumps and ubiquitous changes of L/I with Φ .

The coherent addition of proper modal waves (m_1 and m_2) implies that the observed PA should be at $\psi = 45^\circ$ (with respect to the proper wave PA) whenever the lag distribution is wide and the modes' amplitudes are equal.¹³ Note that such statistical average of signals with different $\Delta\phi$ reproduces the PA value that would be expected for a coherent sum of linearly polarized modal waves at zero lag, ie.:

$$\psi = \psi_{in} = \arctan(E_2/E_1). \quad (22)$$

This equation is valid for other amplitude ratio values, however, for the full uniform distribution of β the PA maxima

¹³ For a narrow $N_{\Delta\phi}$ the observed PA becomes determined by an accidental value of $\Delta\phi$ or $\Delta\phi_{pk}$. A wider $N_{\Delta\phi}$ allows for the statistically average value to stand out in a stable way.

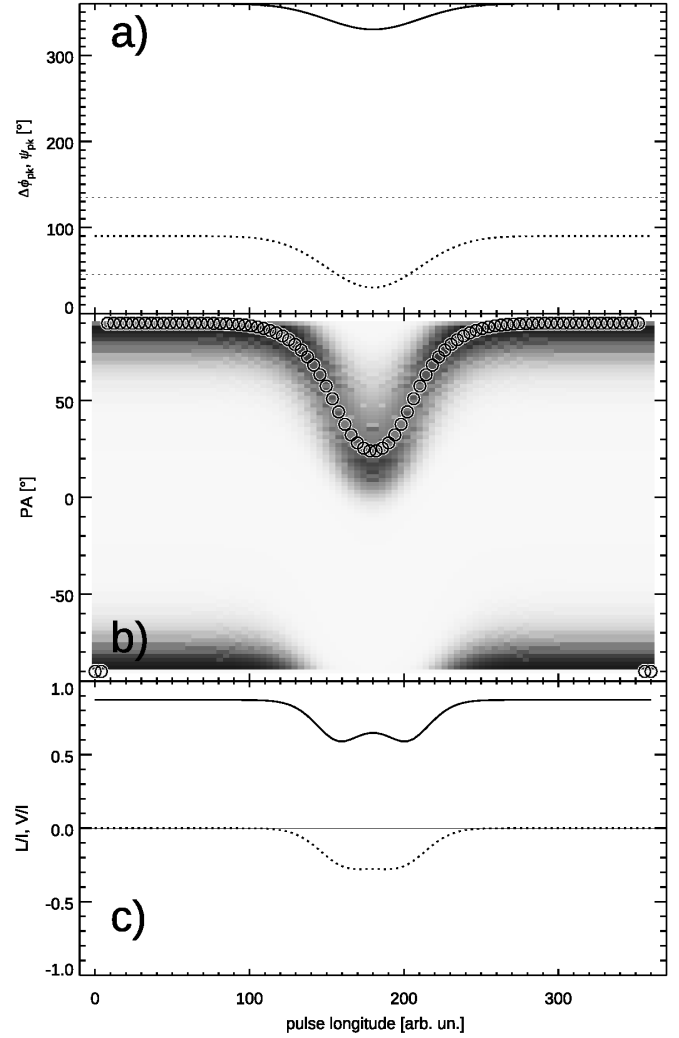


Figure 24. Same as in the previous figure, but for a smaller amplitude of the lag deviation (see the solid line in a). The PA loop has been transformed into the U-shaped PA distortion similar to that observed in B1933+16 at 4.5 GHz. L/I and V/I also change in the way consistent with the data.

appear as two pairs, visible in the right panels of Figs. 19 and 20, ie. they appear at $\psi = \pm\psi_{in}$, and $\psi = 90^\circ \pm\psi_{in}$. For a narrower distribution of eccentricities only some of these four peaks remain in the signal. Fig. 22 is calculated for uniform β in the range $(0, 45^\circ)$ and $\psi_{in} = 30^\circ$ (hence this case is a subpart of Fig. 19). This gives two PA tracks at $\pm\psi_{in}$, ie. separated by 60° . The phenomenon of non-orthogonal PA tracks is often observed in radio pulsar data. For example, in PSR B1944+17 and PSR B2016+28 (Fig. 15 in MAR15) the PA tracks are neither orthogonal nor parallel, which requires the nonequal modal amplitude to change with Φ .

7.5.2 Off-RVM PA wandering

For increasingly non-equal amount of modes, ψ will diverge from 45° and, in the limit of one mode absent, the observed PA must become equal to 0 or 90° , ie. it must start to coincide with one of the natural modes. Therefore, the model predicts that whenever the mode ratio is changing (along

with changing Φ or ν) between 1 and 0, the observed PA should exhibit transitions between the observed intermodal PA track (at $\psi = 45^\circ$) and the proper mode at $\psi = 0$. In a general case, the PA can wander between some initial ψ_{in}^{init} and a final ψ_{in}^{fnl} , with the values determined by their corresponding mode amplitude ratios, as given by eq. (22).

This type of phenomenon likely occurs on the right side of the 660 MHz profile in J0437–4715 (Fig. 4). The ν -dependent modal ratio may also affect the strongly ν -dependent look of polarization within the core component of this pulsar. However, figures 17–22 clearly show that changes of lag with ν can affect the observed polarization at least equally strongly, and in fact they do, as is shown in the following section.

7.6 Frequency dependent lag and the loop of B1933+16

The OPMs observed to the left of the PA loop in PSR B1933+16 are stable at different frequencies: they look as the same pair of orthogonal patches at both 1.5 and 4.5 GHz (see Fig. 1 in MRA16). This holds despite the ratio of observed OPMs quickly changes with pulse longitude Φ at both frequencies. The steady orthogonal location of the modes can be ensured both in the linear-fed model of Fig. 5 and in the circular-fed model of Fig. 7. In the case of the coproper modes of D17, the lag distribution must be wide so that the nodes at PA of 0 and 90° are enhanced. For a narrow $\Delta\phi$ distribution the proper modal waves m_1 and m_2 would coherently combine to an arbitrary PA, as given by eq. (22). Alternatively, the proper modal waves would have to be detected non-simultaneously (to avoid coherent addition) to hold the steady PA at 0 and 90° .

The observed minima in L/I of B1933+16 (Fig. 1 in MRA16) reveal that the mode amount ratio is being inverted every 4° or so in the profile, so it is natural to assume that R temporarily becomes close to unity ($\psi_{in} = 45^\circ$ or 135°) within the loop (where ‘temporarily’ again means ‘within the narrow interval of Φ ’). Therefore, it is assumed in the following that ψ_{in} slightly crosses the value of 45° within the PA loop. For simplicity, the eccentricity is set to infinity (linear waves, $\beta = 0$) so that the model considered is that of Fig. 5 (which is a special case of the general model shown in Fig. 16). Moreover, since changes of $\Delta\phi$ appear indispensable to obtain the bifurcation effect, it is assumed that both ψ_{in} and $\Delta\phi$ change within the loop.

Fig. 23 presents polarization characteristics calculated for the Gaussian change of ψ_{pk} and $\Delta\phi_{pk}$, as shown in panel a with the dotted and dashed line, respectively. Both Gaussians have the pulse longitude width $\sigma = 30^\circ$. The values of $\sigma_{\psi_{in}} = 15^\circ$ and $\sigma_{\Delta\phi} = 45^\circ$ are fixed across the pulse window. Outside the loop the modelled PA track follows the proper mode at $\psi = 90^\circ$, because the assumed profile for the peak of the mixing angle distribution is: $\psi_{pk} = 90^\circ - 60^\circ \exp(-0.5(\pi - \Phi)^2/\sigma^2)$. When ψ_{pk} diverges from 90° so much that the intermode is crossed (dotted horizontal at 45°) the PA loop is opened on the coproper OPM track.¹⁴ The loop is not identical to the observed one, but

¹⁴ It is therefore not necessary for the OPMs left to the loop to be intermodal.

several observed features are reproduced: there are upward-pointing ‘horns’ of PA at the top of the loop, little power inside the loop, and the bottom of the loop extends into the downward-pointing tongue of radiative power that reaches all the way to the top of the loop (after the PA axis is wrapped up with the 180° period). The twin minima in L/I and the single-sign V are also well reproduced.

The simultaneous changes of $\Delta\phi$ seem to be indispensable in this model. The change of ψ_{in} alone does not produce the bifurcation, and the result in such case resembles that of Fig. 11 in D17.

The profile of peak value in the lag distribution was $\Delta\phi_{pk} = 360^\circ - 100^\circ \exp(-0.5(\pi - \Phi)^2/\sigma^2)$, ie. the amplitude of the lag change is equal to 100° in Fig. 23. When the lag-change amplitude is decreased to 30° , the result of Fig. 24 is obtained. One can see that the loop disappears and is transformed into the U-shaped PA distortion, much like the one observed in the data at 4.5 GHz (Fig. 1 in MRA16). Moreover, the twin minima in L/I become shallower, but do not merge, again as observed for B1933+16. The value of L/I increases, while $|V|/I$ decreases, in agreement with data at both 1.5 GHz and 4.5 GHz.

The decrease of lag amplitude is thus the only thing which is needed to understand the evolution of the PA loop with frequency. It is possible to obtain the right behaviour with the decrease of lag only, which is naturally expected at the increased ν .

The phase lag may be a strong function of ν and it is possible that $\Delta\phi$ becomes negligible at 4.5 GHz. If so, then the observed PA track of the U-shaped distortion directly reveals the profile of ψ_{pk} , which is indeed observed to be about 45° away from the OPMs that are observed outside the loop (the dotted curve in Fig. 24a is reproduced in the PA curve of Fig. 24b, to be compared with the 4.5 GHz data in Fig. 1 of MRA16).

The result of this section again shows that the core polarization of pulsars is a combination of amplitude-driven and lag-driven effects, and the look of PA curves and other polarization characteristics change with frequency, because of the frequency-dependent phase lag. When the Gaussian profiles of $\psi_{pk}(\Phi)$ and $\Delta\phi_{pk}(\Phi)$ are misaligned, the resulting profiles of L/I and V/I become asymmetric, which is observed at both frequencies. It should be possible to construct a similar multifrequency model for the complex behaviour of core polarization in J0437–4715 at different frequencies.

It must be noted that several effects of the lag change can also be produced through the narrowing of $N_{\Delta\phi}$ distribution. For example, a result similar to that of Fig. 23 can be obtained for a fixed (Φ -independent) $\Delta\phi_{pk}$ when $\sigma_{\Delta\phi}$ is changing within the loop. Reasonably looking loops were in particular obtained for a one-sided $N_{\Delta\phi}$ with $\sigma_{\Delta\phi}$ following the profile of $\sigma_{\Delta\phi} = 145^\circ - 135^\circ \exp(-0.5(\pi - \Phi)^2/\sigma^2)$. In such case the exact shape of the resulting loop depends on the $\Delta\phi_{pk}$ value.

7.7 Lag-driven inversions of PA distortions

Polarization characteristics that result from coherent mode addition sometimes are very sensitive to the parameters used. The results illustrated in the previous section were calculated for symmetric (two-sided) lag distribution $N_{\Delta\phi}$. Fig. 25 presents a different result for a one-sided $N_{\Delta\phi}$. The

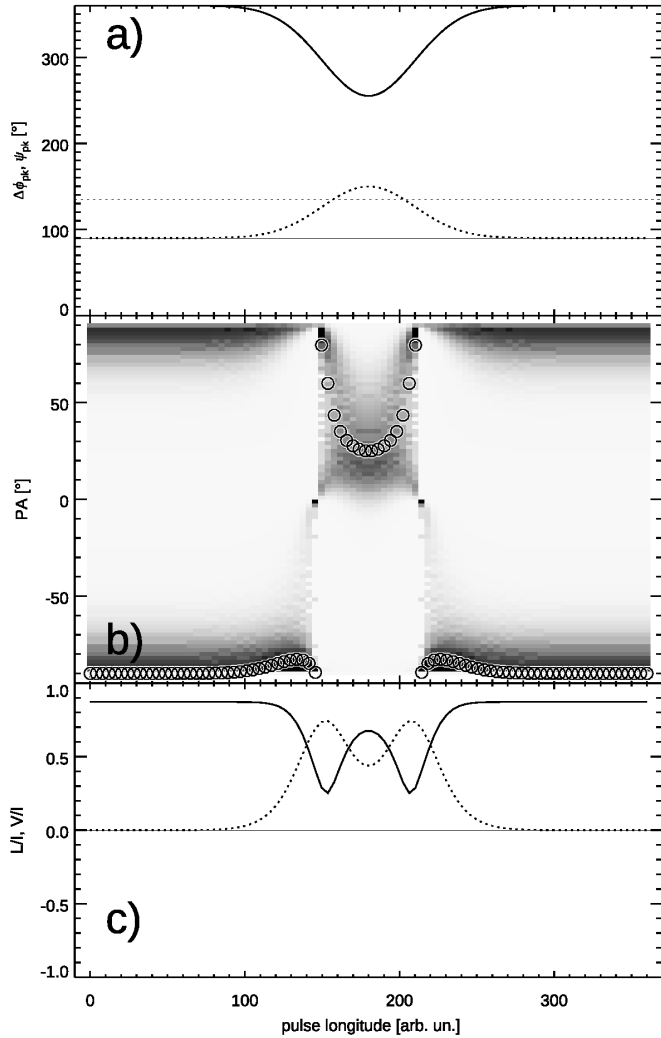


Figure 25. Polarization characteristics calculated for the ψ_{pk} and $\Delta\phi_{pk}$ profiles shown in panel **a**, and for $\sigma_{\psi, in} = 15^\circ$, $\sigma_{\Delta\phi} = 45^\circ$. The PA is distorted downward, and V is positive.

amplitudes of the ψ_{pk} and $\Delta\phi_{pk}$ profiles are 60° and 105° , respectively, and ψ_{pk} now increases within the PA distortion (see the dotted line in panel **a**).

A change of only the lag amplitude to 35° leads to the result of Fig. 26. The PA distortion is now protruding upwards, whereas the other polarization characteristics (such as L/I and V/I do not change much). This phenomenon resembles the PA bifurcation of B1237+25 in the N and Ab modulation states (SRM13). With the change of modulation state, the observed PA follows different branch of the PA bifurcation while the sign of V does not change. It appears possible then, that the exchange of the followed PA branch is caused only by the change of the lag value in different modulation states.

Obviously, the phenomenon of the modulation-state-dependent polarization, and other complex polarization phenomena in pulsars require more detailed study. The parameter space for the coherent addition of non-equal elliptical modes offers a large number of possible polarization profiles. Fig. 27 presents the PA as a function of lag, calculated for a sparse grid of parameters: $\Delta\psi_{in} = 10^\circ$, $\Delta\beta = 5^\circ$, and

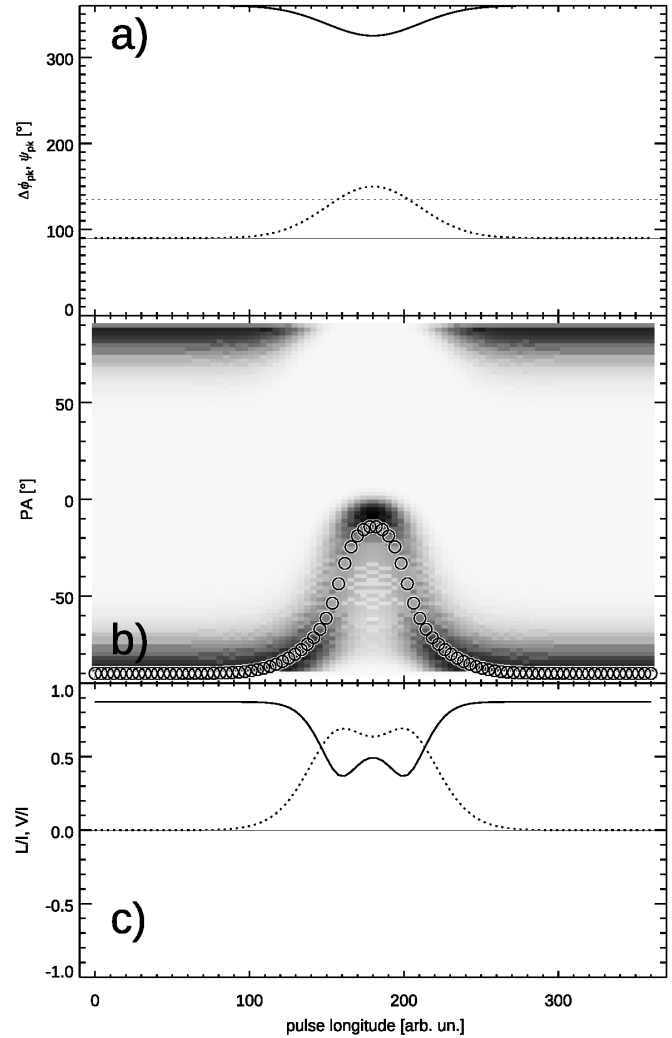


Figure 26. Same as in previous figure, but for a smaller amplitude of the $\Delta\phi_{pk}$ profile (top solid line). The PA is now distorted upward, but the sign of V does not change. This behaviour resembles that observed in the core of B1237+25 in different modulation states (Fig. 1 and 6 in SRM13).

$\Delta(\Delta\phi) = 1^\circ$. Different lines of $\psi(\Delta\phi)$ correspond to different pairs of (ψ_{in}, β) . A numerical code for pulsar polarization needs to probe even larger parameter space, with the added widths of statistical distributions of ψ_{in} , $\Delta\phi$, and β . To make things more complex, it may be necessary to introduce a few additional parameters that describe how these six basic parameters depend on pulse longitude Φ . More complete analysis of the phenomena visible in Fig. 27, along with detailed numerical fitting of pulsar data, is deferred to further study.

8 CONCLUSIONS

It has been shown that complex non-RVM polarization effects in radio pulsars can be understood in geometrical terms, as the result of coherent and quasi-coherent addition of elliptically polarized orthogonal proper-mode waves. The phenomenon of coherent mode addition is described by

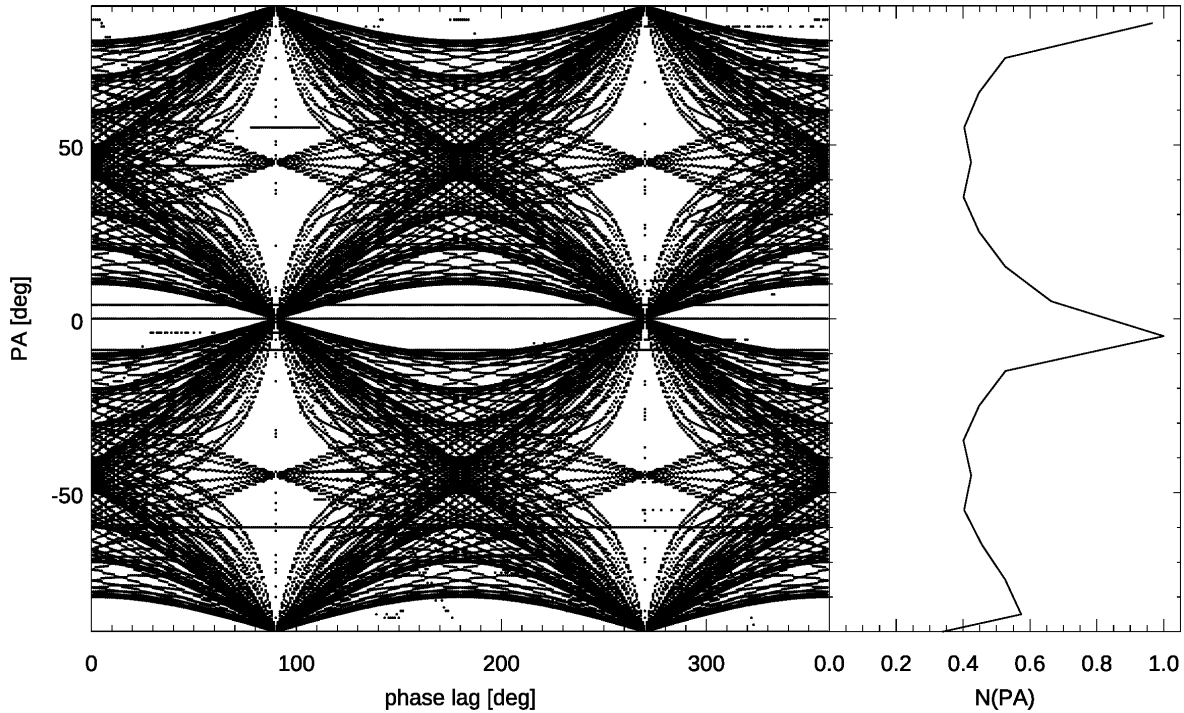


Figure 27. The lag-PA diagram for sparsely and uniformly sampled parameter space of $(\Delta\phi, \psi_{in}, \beta)$. The result has been obtained for intervals: $\Delta(\Delta\phi) = 1^\circ$, $\Delta\psi_{in} = 10^\circ$ and $\Delta\beta = 5^\circ$. The coproper nodes at $\psi = n90^\circ$, the linearly polarized diagonals, and the intermodes at $\psi = 45^\circ + n90^\circ$ seem to stand out most in this picture. For increasing $\Delta\phi$, a radio signal with fixed ψ_{in} and β would have the PA changing along one of the visible lines.

three (or six) parameters: the phase lag, the amplitude ratio (mixing angle), and the eccentricity of polarization ellipse (plus the widths of their distributions). The model implies that the observed radio polarization is driven by at least two independent effects: the changes of mode amplitude ratio, which, in particular, are responsible for the regular OPM behaviour (with zero V at OPM transitions) and the changes of the phase lag which have opposite characteristics. Both these factors influence the observed polarization within the same pulse intervals, which is evident in the core region of profiles. Such model explains several complicated and dissimilar phenomena, such as: distortions, bifurcations and loops of the PA observed in the central part of profiles, twin minima in L/I associated with these distortions, maxima of $|V|/I$ at OPM jumps, 45° -off PA tracks, chaotic spread of PA values within the 45° -displaced emission, and dissimilar L/I minima of mixed origin, such as those observed in J0437–4715. Moreover, the model is capable to interpret the changing look of these phenomena with frequency and possibly with modulation state.

The observed OPM tracks have often been directly associated with the natural propagation mode waves. It has been shown here that the observed OPMs do not necessarily correspond to the natural waves. Instead, the observed OPMs are a statistical average of coherent sum of the natural waves (with diverse phase lags). Therefore, the PA of observed polarization tracks can be completely different from the PA of the natural waves. The observed PA tracks may be non-orthogonal and they may wander away from the RVM PA. The coherent addition model implies that the PA is distorted by the ν -dependent location and width of the lag distribu-

tion, and by the ν -dependent ratio of modal amplitude, as expressed by eq. (22).

In the noncoherent model the observed PA can only jump by 90° when one mode becomes stronger than another. In the coherent mode addition model, the noncoherent condition is obtained by coherent summation of numerous natural mode waves at diverse phase lags. This typically causes the coproper modes M_1 and M_2 to stand out in the data. Preference of equal modal amplitudes, however, makes the intermodes C_1 and C_2 most pronounced.

Identical amplitudes of the natural propagation mode waves (m_1 and m_2) are automatically produced when the waves are fed by a circularly polarized signal. The coherent addition model then implies that two pairs of observed OPM tracks may in general appear in pulsar profiles, and the pairs are separated by 45° . Just like the linear-fed coproper modes, the intermodal OPMs are pronounced when the phase lag distribution is wide, which introduces many polarization ellipses that all share the same PA of 45° (or -45° , see Fig. 7).

In the case of the linear-fed coproper modes, the pseudomodal OPM jumps are produced when ψ_{in} is passing through the intermodal value of 45° . $|V|/I$ is maximum at such OPM transitions. In the case of the circular-fed equal-amplitude OPMs, the regular OPM jumps take place when the handedness of the feeding wave is changed. In the case of the general model with the elliptical proper modes, the regular OPM jumps occur in the usual way (when one mode becomes stronger than another, for whatever reason).

When the mode amplitude ratio slowly deviates from 1, the observed PA makes a non-orthogonal passage between

the intermodal PA value and the natural mode PA, eg. between 45° and 90° . Such change of PA does not have to be precisely equal to 45° given the possible simultaneous change of PA caused by the RVM effect. Examples of such slow wandering of PA between the OPM values can often be found in pulsar data, eg. on the trailing side of profile in J0437–4715, Fig. 4.

The presented model solves several problems that appeared in the analysis of D17. The complex polarization in the core components of both normal and millisecond pulsars can be understood as the result of simultaneous changes of phase lag (with pulse longitude and frequency) and of the mode amount ratio (which changes at least with pulse longitude). The change of lag with ν is responsible for the different look of the PA loop in B1933+16 at 1.5 and 4.5 GHz. If the profiles of lag and mode ratio are misaligned in pulse longitude, it is possible to produce the dissimilar twin minima in L/I as observed in J0437–4715. The original two-parameter lag-PA diagram of D17 seemed to clearly indicate where the observed OPMs are located, but it is found here that the observed ‘modes’ (PA tracks) in general do not coincide with the natural modes. They can be at any distance from the RVM PA, they can be non-orthogonal, and they can be intermodal wherever the amplitude ratio is close to unity.

The result of Fig. 23 shows that a fairly simple underlying model (see the Gaussian profiles in top panel) can produce the very complex effect of the PA loop (panel b). The coherent mode addition thus presents a capable interpretive tool. However, the model contains many parameters: at least the lag, mixing angle, widths of their distributions, plus six parameters for their pulse-longitude dependence (amplitude, peak longitude, and the width, in the case of a Gaussian). Even with the ellipticity ignored, this makes up for ten free parameters. Moreover, some pairs of the parameters (such as the lag and mixing angle, or the peak lag value and the width of the lag distribution) are degenerate at least to some degree. Therefore, it is not easy to find the best fit parameters through a hand-made sampling of the parameter space. Neither it is easy to break the degeneracy. A possible way out is to consider the ν dependence of modelled phenomena, which has helped us to break the ψ_{in} - $\Delta\phi$ degeneracy in the case of the loop in B1933+16. Modelling of the single pulse data (distributions of PA, L/I and V/I at a fixed Φ) may also prove useful. A need for a carefully designed fitting code is apparent.

ACKNOWLEDGEMENTS

I thank Richard Manchester for the average pulse data on J0437–4715 (Parkes Observatory). Plotting of polarized fractions for B1919+21 was possible thanks to the public Arecibo Observatory data base provided by Dipanjan Mitra, Mihir Arjunwadkar, and Joanna Rankin (MAR15). I appreciate comments on the manuscript from Bronek Rudak, discussions with Adam Frankowski and I thank Wolfgang Sieber for words of encouragement. This work was supported by the grant 2017/25/B/ST9/00385 of the National Science Centre, Poland.

9 APPENDIX

REFERENCES

- Brinkman C., Freire P. C. C., Rankin J., Stovall K., 2018, MNRAS, 474, 2012
- Dyks J., 2017, MNRAS, 472, 4617 (D17)
- Edwards R. T., 2004, A&A, 426, 677
- Edwards R. T., Stappers B. W., 2003, A&A, 410, 961
- Edwards R. T., Stappers B. W., 2004, A&A, 421, 681
- Everett J. E., Weisberg J. M., 2001, ApJ, 553, 341
- Gangadhara R. T., 2010, ApJ, 710, 29
- Hankins T. H., Rankin J. M., 2010, AJ, 139, 168
- Johnston S., Kerr M., 2018, MNRAS, 474, 4629
- Karastergiou A., 2009, MNRAS, 392, L60
- Lyubarskii Y. E., Petrova S. A., 1998, Astrophysics and Space Science, 262, 379
- McKinnon M. M., 2003, ApJ, 590, 1026
- McKinnon M. M., Stinebring D. R., 1998, ApJ, 502, 883
- McKinnon M. M., Stinebring D. R., 2000, ApJ, 529, 435
- Melrose D., Miller A., Karastergiou A., Luo Q., 2006, MNRAS, 365, 638
- Melrose D. B., 1979, Australian Journal of Physics, 32, 61
- Michel F. C., 1991, Theory of neutron star magnetospheres. University of Chicago Press
- Mitra D., Arjunwadkar M., Rankin J. M., 2015, ApJ, 806, 236 (MAR15)
- Mitra D., Rankin J., Arjunwadkar M., 2016, MNRAS, 460, 3063 (MRA16)
- Mitra D., Rankin J. M., 2008, MNRAS, 385, 606
- Navarro J., Manchester R. N., Sandhu J. S., Kulkarni S. R., Bailes M., 1997, ApJ, 486, 1019
- Noutsos A., Sobey C., Kondratiev V. I., Weltevrede P., Verbiest J. P. W., Karastergiou A., Kramer M., et al. 2015, A&A, 576, A62
- Oslowski S., van Straten W., Bailes M., Jameson A., Hobbs G., 2014, MNRAS, 441, 3148
- Rafat M. Z., Melrose D. B., Mastrano A., 2018, arXiv e-prints
- Rankin J. M., Archibald A., Hessels J., van Leeuwen J., Mitra D., Ransom S., Stairs I., van Straten W., Weisberg J. M., 2017, ApJ, 845, 23
- Rankin J. M., Ramachandran R., 2003, ApJ, 590, 411
- Smith E., Rankin J., Mitra D., 2013, MNRAS, 435, 2002 (SRM13)
- Wang C., Lai D., Han J., 2010, MNRAS, 403, 569
- Young S. A. E., Rankin J. M., 2012, MNRAS, 424, 2477

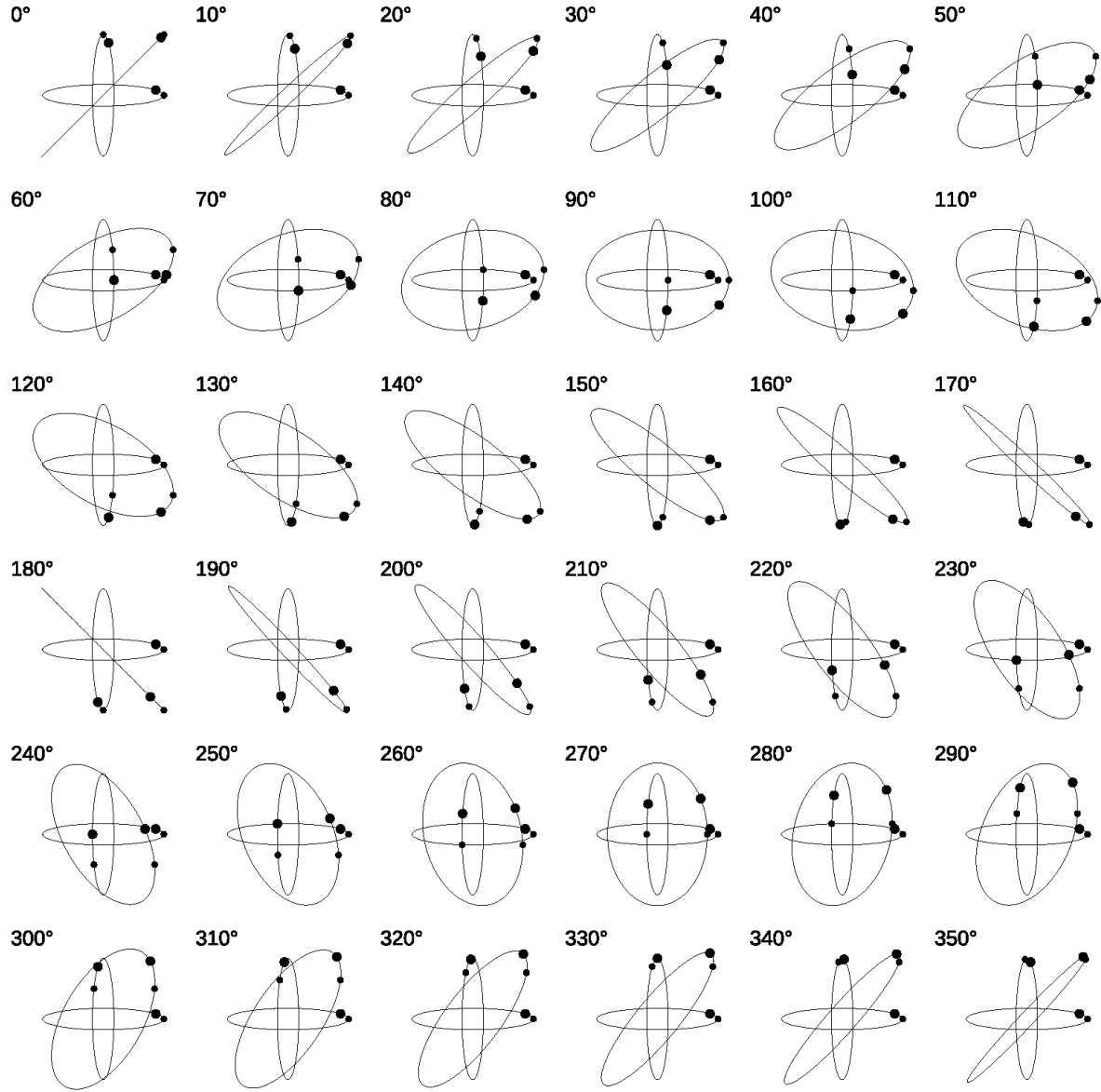


Figure 28. Coherent summation of two orthogonal elliptically polarized natural propagation mode waves (narrow orthogonal ellipses). Numbers in the corners give the value of phase lag used in the summation. The result has the form of a wide ellipse, a narrow ellipse at nearly diagonal orientation, or a diagonal line (linear polarization at $\Delta\phi = 0$ and 180°). For most lag values the result has the PA close to $\pm 45^\circ$. Only in the second and fifth horizontal row the PA deviates considerably from $\pm 45^\circ$. The dots on the ellipses refer to the same moment of time (t_1 for small dots, $t_2 > t_1$ for the large dots, i.e. the direction of electric field circulation is from a small dot to a large one). The eccentricity angle of the ellipses that are added is $\beta = 10^\circ$. The result roughly corresponds to the S-shaped lines in Fig. 17 and 18, i.e. it is not far from the discontinuous case with the PA jumping from 45° to -45° at $\Delta\phi = 90^\circ$ (and back at 270°).

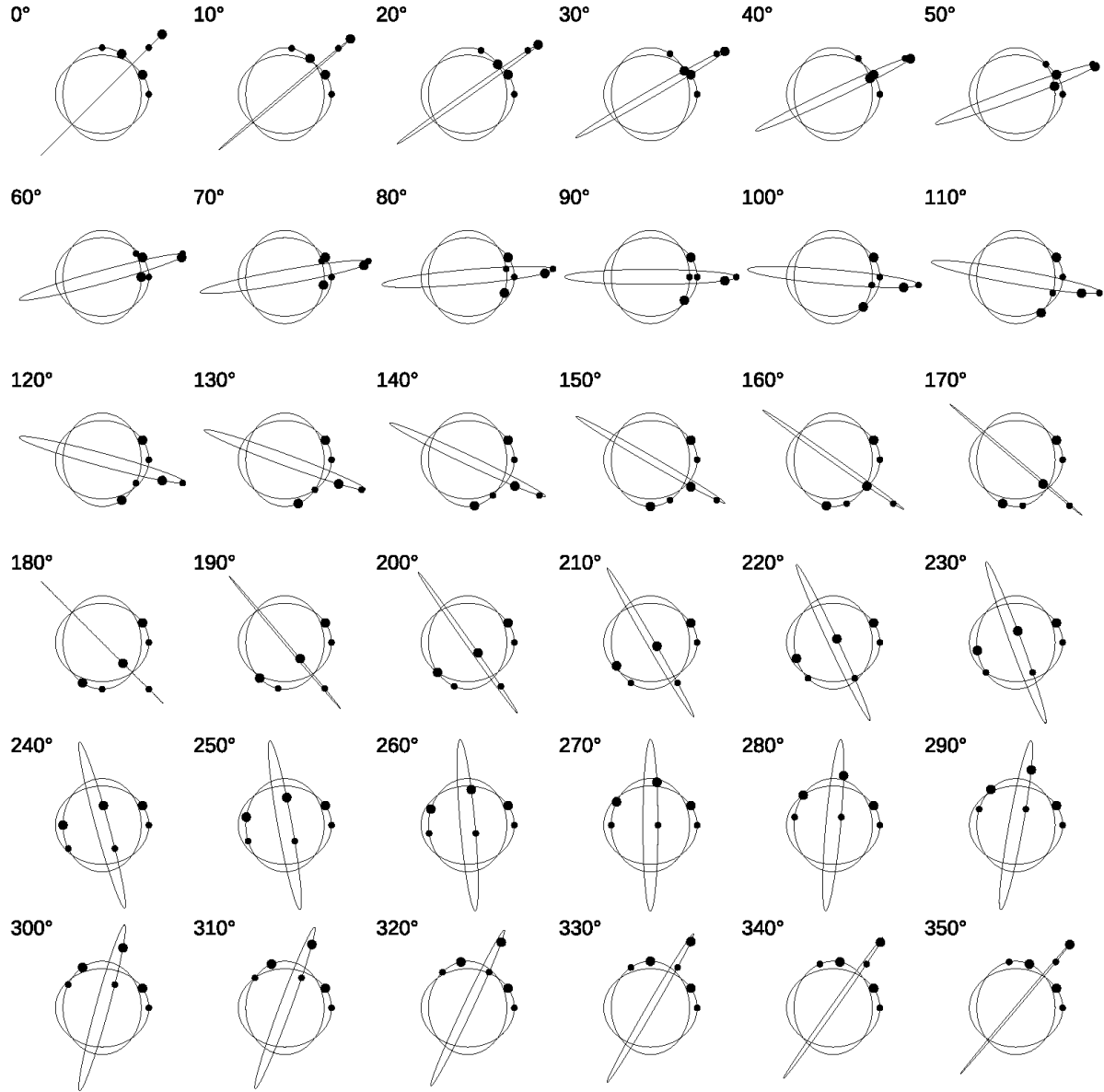


Figure 29. Same as in previous figure, but for nearly circularly polarized natural waves ($\beta = 40^\circ$). This case is close to the diagonals shown in Figs. 17 and 18, i.e. the PA of the resulting wave increases almost uniformly as in the Faraday rotation effect.